Pharmacological Research 211 (2025) 107554

Contents lists available at ScienceDirect

Pharmacological Research

journal homepage: www.elsevier.com/locate/yphrs

Unveiling the link between NADPH oxidase 2 activation and mitochondrial superoxide formation in leukemic cell killing induced by arsenic trioxide

Andrea Spina [1,1], Andrea Guidarelli [1], Gloria Buffi, Mara Fiorani, Orazio Cantoni [*]

Department of Biomolecular Sciences, University of Urbino Carlo Bo, Urbino, Italy

ARTICLE INFO

Keywords:
Arsenic trioxide
NADPH oxidase 2-derived superoxide
Mitochondrial superoxide
Mitochondrial permeability transition
Apoptosis

ABSTRACT

This study focused on the interplay between NADPH oxidase 2 (NOX 2) activation and mitochondrial superoxide ($mitoO_2^{\cdot-}$) formation induced by clinically relevant concentrations of arsenic trioxide (ATO; As_2O_3) in acute promyelocytic leukemia (APL) cells.

Carefully controlled inhibitor studies and small interfering RNA mediated downregulation of $p47^{phox}$ (a component of the NOX 2 complex) expression demonstrated that, in an APL cell line, ATO promotes upstream NOX 2 activation critically connected with the formation of $mitoO_2^{\cdot-}$ and with the ensuing mitochondrial permeability transition (MPT)-dependent apoptosis.

Instead, acute myeloid leukemia (AML) cell lines respond to ATO with low NOX 2 activation, resulting in a state that is non-permissive for $mitoO_2^{\cdot-}$ formation. Consistently, through rescue experiments, we demonstrate that pharmacological stimulation of NOX 2 overcomes resistance in these cells, thereby initiating the same cascade of downstream events observed in APL cells.

As a final note, several lines of evidence, including measurement of glutathione, catalase and glutathione peroxidase levels, indicated that the antioxidant machinery was similar in APL and AML cells. The results regarding nuclear factor erythroid 2 p45-related factor 2-dependent antioxidant responses were instead of more complex interpretation as NB4 cells appeared particularly responsive to ATO.

Our findings allow a novel interpretation of the interplay between NOX 2 activation and $mitoO_2^{\cdot-}$ formation induced by ATO, ultimately steering leukemic cells towards MPT-dependent apoptosis. These mechanistic insights provide a rationale for the disparate responses of APL and AML cells to ATO, offering potential avenues for the development of therapeutic intervention tailored to specific leukemia subtypes.

1. Introduction

Arsenic trioxide (ATO; As_2O_3) is characterized by relatively manageable side effects, and is currently employed in the treatment of some hematological malignancies and other selected human cancers [1–6]. In particular, acute promyelocytic leukemia (APL) is sensitive to ATO monotherapy [7,8], possibly due to the expression of APL-specific promyelocytic leukemia-retinoic acid receptor-α (PML/RARα) fusion protein [9–12], which contributes to the induction of differentiation and apoptosis [6,10,11,13,14]. ATO has revolutionized APL treatment, which was previously associated with poor prognosis [11,12].

Although promoting an array of effects, as inhibition of angiogenesis [15,16], immunomodulation [17], inhibition of enzymatic activities [18] and interference with various signaling pathways [12,16], which contribute to its potent antitumoral activity, ATO causes the formation of reactive oxygen species (ROS), considered of pivotal importance for the induction of apoptosis [19–22]. APL susceptibility to ATO, detected also in *in vitro* studies using APL cell lines (e.g., NB4 cells), has been

Abbreviations: AML, acute myeloid leukemia; APL, acute promyelocytic leukemia; ATO, As_2O_3, arsenic trioxide; ATZ, 3-amino-1,2,4-triazole; BSA, bovine serum albumin; CsA, cyclosporin A; DHR, dihydrorhodamine 123; DPI, diphenyleneiodonium; EDTA, ethylenediaminetetraacetic acid; FBS, fetal bovine serum; GPx, glutathione peroxidase; H_2O_2, hydrogen peroxide; $MitoO_2^{\cdot-}$, mitochondrial superoxide; MPT, mitochondrial permeability transition; NAO, 10-N-nonyl acridine orange; NOX 2, NADPH oxidase 2; NQO1, NADPH:quinone oxidoreductase 1; NPSH, Non-protein thiols; Nrf2, nuclear factor erythroid 2 p45-related factor 2; PBS, phosphate buffer saline; PMA, phorbol-12-myristate-13-acetate; PML/RARα, promyelocytic leukemia-retinoic acid receptor-α; ROS, reactive oxygen species.

* Correspondence to: Dipartimento di Scienze Biomolecolari, Sezione di Farmacologia e Farmacognosia, Università degli Studi di Urbino, Via S. Chiara 27, Urbino, PU 61029, Italy.

E-mail address: orazio.cantoni@uniurb.it (O. Cantoni).

[1] These authors contributed equally to this work.

https://doi.org/10.1016/j.phrs.2024.107554
Received 29 August 2024; Received in revised form 6 December 2024; Accepted 13 December 2024
Available online 16 December 2024

associated with their significant ROS response [19,22,23].

Numerous studies have demonstrated that clinically relevant ATO concentrations, i.e., $\leq$ 2 μM [24–26], promote the formation of ROS in the mitochondrial respiratory chain of susceptible cells, an event followed by the onset of mitochondrial dysfunction and mitochondrial permeability transition (MPT) dependent release of pro-apoptotic factors, as cytochrome c, and by the ensuing activation of the apoptotic cascade [20,27,28]. This mechanism of cell death is considered particularly important in the context of ATO induced apoptosis in APL cells [20,27,28].

Another critical mechanism whereby ATO induces ROS formation, is associated with the activation of NADPH oxidase 2 (NOX 2, [23,29–31]), a multi-subunit enzyme complex localized in the plasma membrane [32], which catalyzes the transfer of electrons from NADPH to molecular oxygen, thereby generating superoxide anions ($O_2^{\cdot-}$). The formation of these species has also been associated with the triggering of toxic events leading to apoptosis [31,33]. It has been proposed that the elevated susceptibility of APL cells to ATO is associated with their significant responsiveness in terms of NOX 2 dependent ROS formation [23,29,30]. This specific susceptibility is partially explained by the ability of ATO to increase the expression of $p47^{phox}$ and of other NOX 2 components [23], and to an effect of the PML/RARα fusion protein on cAMP levels, which leads to NOX 2 hyperactivation [29].

However, the specific role of NOX 2 derived ROS in MPT dependent apoptosis induced by ATO remains elusive. Also unclear is whether this and the mitochondrial mechanisms of ROS formation are independent of interconnected processes.

Acute myeloid leukemia (AML), unlike APL, is resistant to ATO alone and several strategies have been exploited to enhance its toxicity in these hematological malignancies [34–38]. AML cell lines widely employed in laboratory studies, as U937 or THP-1 cells, while not expressing the PML/RARα fusion protein, are poorly responsive in terms of ROS release and toxicity when exposed to concentrations of ATO $\leq$ 2 μM [27–29,39]. Significant mitochondrial and NOX 2 dependent ROS formation and toxicity is instead induced by remarkably greater, clinically irrelevant ATO concentrations, an observation suggesting that these cells display more efficient antioxidant defenses and/or reduced ROS formation *via* either one or both of the above mechanisms [27,30,40].

Unfortunately, these resistance mechanisms are poorly understood because of the limited knowledge of some critical details concerning the regulation of the overall oxidative stress response generated by ATO in sensitive and resistant cells. Given the specific relevance of $mitoO_2^{\cdot-}$ in ATO induced apoptosis [20,41], it is important to learn more on the mechanisms regulating its formation in sensitive cells, to then attempt to circumvent the resistance mechanism of AML cells *via* pharmacological modulation.

In this study, we employed concentrations of ATO $\leq$ 1 μM to elucidate the relationship(s) existing between NOX 2 activation and $mitoO_2^{\cdot-}$ formation, under conditions associated with the triggering of MPT-dependent apoptosis in sensitive NB4 cells [27,40]. Interestingly, NOX 2 activation was upstream to, and critically connected with, the formation of $mitoO_2^{\cdot-}$, and hence with the triggering of the mitochondrial pathway of apoptosis. Under the same conditions, $mitoO_2^{\cdot-}$ emission and MPT-dependent apoptosis were not detected in AML cell lines, which displayed baseline antioxidant defense like that of NB4 cells. The resistance phenotype of U937 and THP-1 cells was apparently associated with their low release of NOX 2 derived ROS, insufficient to activate events leading to $mitoO_2^{\cdot-}$ formation. Thus, AML cells responded to ATO and pharmacological stimulation of NOX 2 with significant $mitoO_2^{\cdot-}$ formation. Furthermore, under these conditions, the cells underwent the same sequence of downstream events detected in APL cells.

2. Materials and methods

2.1. Chemicals

ATO, $NaAsO_2$, rotenone, apocynin, diphenyleneiodonium (DPI), phorbol-12 myristate-13-acetate (PMA), Hoechst 33342, 3-amino-1,2,4-triazole (ATZ), as well as most of the reagent end chemicals, were purchased from Sigma Aldrich (Milan, Italy). Cyclosporin A (CsA) was from Novartis (Bern, Switzerland). Dihydrorhodamine 123 (DHR) and MitoSOX red were purchased from Thermo Fisher Scientific (Milan, Italy). 10-N-nonyl acridine orange (NAO) and MitoTracker red CMXRos were purchased from Molecular Probes (Leiden, The Netherlands).

ATO was dissolved in 1 N NaOH, diluted in phosphate buffer saline (PBS, 136 mM NaCl, 10 mM Na_2HPO_4, 1.5 mM KH_2PO_4, 3 mM KCl; pH 7.4), and adjusted to pH 7.4 using HCl, to generate a 10 mM solution which was further diluted in PBS to generate a 1 mM stock solution, which was kept at 4 °C for up to three days. Working solutions were freshly prepared from the stock solution by dilution in cell culture medium on the day of the experiment.

$NaAsO_2$ was prepared as a 1 mM stock solution in PBS and stored at 4 °C. Cells were exposed to ATO, $NaAsO_2$ and/or other additions in complete RPMI 1640 culture medium.

In experiments involving catalase depletion, the U937 cells (5×10^6/20 ml) were incubated for 6 h at 37°C in RPMI medium containing 10 mM ATZ, an irreversible inhibitor of catalase [42]. Experiments with H_2O_2 were performed in 2 ml of saline A (8.182 g/l NaCl, 0.372 g/l KCl, 0.336 g/l $NaHCO_3$ and 0.9 g/l glucose) containing 5×10^5 cells.

2.2. Antibodies

The antibody against $p47^{phox}$ (SAB4502810) was purchased from Merk (Merk chemicals, DE), and the antibody against phospho-$p47^{phox}$ (Ser345) (PA5–37806) was purchased from Invitrogen (Thermo Fisher Scientific). The antibody against nuclear factor erythroid 2 p45-related factor 2 (Nrf2) (#12721) and NAD(P)H:quinone oxidoreductase 1 (NQO1) (#3187) was purchased from Cell Signalling Technology (EuroClone, Milan, Italy). The antibody against β-actin (VMA00048) was purchased from Bio-Rad (Hercules, CA). The antibody against GADPH (CPA9067) was purchased from Cohesion (CliniSciences Italy, Rome, Italy). The antibody against cytochrome c (sc-13560), horseradish peroxidase-conjugated mouse (sc-516102) secondary antibodies, horseradish peroxidase-conjugated rabbit (sc-2357) secondary antibodies, and fluorescein isothiocyanate-conjugated polyclonal goat anti-rabbit (sc-2359) or anti-mouse (sc-516140) antibodies were purchased from Santa Cruz Biotechnology (Santa Cruz, CA).

2.3. Cell cultures

ATO resistant AML cell lines, U937 (pro-monocytic human myeloid leukemia) and THP-1 cells (human monocytic leukemia), and the ATO sensitive APL cell line, NB4 cells (human pro-myelocytic leukemia), were cultured in RPMI 1640 medium (Sigma-Aldrich, Milan, Italy) supplemented with 10 % fetal bovine serum (FBS, Euroclone, Celbio Biotecnologie, Milan, Italy). Culture media were supplemented with penicillin (100 units/ml) and streptomycin (100 μg/ml) (Euroclone) and cells were grown at 37 °C in T-75 tissue culture flasks (Corning Inc., Corning, NY) gassed with an atmosphere of 95 % air-5 CO_2.

2.4. Transfection of NB4 cells with siRNA

NB4 cells were transfected with a pool of 4 target-specific $p47^{phox}$ siRNAs (sc-29422, Santa Cruz Biotechnology). Negative controls were instead obtained by transfecting siRNA consisting of a scrambled sequence (sc-36869, Santa Cruz Biotechnology). Transfection procedures followed the manufacturer's instructions. Briefly, 2×10^5 cells/wells were grown to 50–70 % confluence in antibiotic-free media

containing 10 % FBS. Transfection with siRNAs was performed with Transfection Reagent (sc-29528, Santa Cruz Biotechnology), using a final $p47^{phox}$ siRNA or control siRNA concentration of 60 pmols. After 7 h of incubation, the cells were supplemented with RPMI 1640 with FBS and penicillin/streptomycin without removing the transfection mixture. At 48 h after transfection, cells were employed for experiments. The protein levels of $p47^{phox}$ were determined by Western-blot analysis.

2.5. MitoSOX red and DHR fluorescence assay

Cells were grown in 35 mm tissue culture dishes and exposed for 30 min with 5 μM MitoSOX red prior to the end of the 6 h treatment with ATO, or $NaAsO_2$. This fluorogenic dye allows the detection of $O_2^{\cdot-}$ in the mitochondria of live cells [43]. It is indeed readily taken up by the mitochondria *via* a mechanism driven by mitochondrial membrane potential and, in these organelles, reacts with $O_2^{\cdot-}$ thereby generating a red signal that can be detected and quantified using fluorescence microscopy. In some experiments, MitoSOX red was replaced with 10 μM DHR, which, under the influence of various types of ROS, including hydrogen peroxide (H_2O_2), is oxidized in the cytosol and converted to rhodamine 123, a cationic fluorescent dye that is also accumulated in the mitochondria *via* a mitochondrial membrane potential-dependent mechanism. The corresponding fluorescent signal can also be detected by fluorescence microscopy and provides an estimate of ROS formation in the cytosol and mitochondrial origin. Indeed mito$O_2^{\cdot-}$ dismutates to H_2O_2, which eventually reaches extramitochondrial compartments and oxidizes DHR. Thus, both assays require an intact mitochondrial membrane potential. We therefore measured ROS formation under conditions in which the mitochondrial membrane potential, determined as indicated below, resulted unaffected by the specific treatment. Additional information in this direction is provided in the results section.

In some experiments, the cells were exposed for 15 min to DHR and subsequently treated for further 15 min with PMA. The cells were finally washed three times, and the fluorescence images were visualized using a fluorescence microscope.

The excitation and emission wavelengths were 488 and 525 nm (DHR) and 510 and 610 nm (MitoSOX red), with a 5-nm slit width for both emission and excitation. Images were collected with exposure times of 100–400 ms, digitally acquired, and processed for fluorescence determination at the single cell level by ImageJ software. Mean fluorescence values were determined by averaging the fluorescence values of at least 50 cells/treatment condition/experiment.

2.6. Western blot analysis

After treatments, the cells were lysed with RIPA buffer (Thermo Fisher Scientific), with the further addition of 1 mM dithiothreitol, 10 mM Na_3VO_4, 10 mM NaF, 350 mM phenylmethylsulphonyl fluoride, 1 % protease inhibitor complex, pH 7.5. Protein concentrations were determined with the Bradford reagent (Bio-Rad) in SPECTRA Fluor Plus Microplate Reader Tecan (Tecan, CH). The proteins were separated by polyacrylamide gel vertical electrophoresis and transferred to polyvinylidene difluoride membranes. The membranes were blocked in 5 % milk and probed with primary antibodies overnight, at 4 °C. Membranes were washed 3 times for 10 min/each in Tween-Tris buffered saline and probed with secondary antibodies anti-mouse or anti-rabbit diluted in 5 % milk Tween-Tris-buffered saline for 2 h at room temperature. Antibodies against $p47^{phox}$, GADPH or β-actin were used to assess the equal loading of the lanes. Membranes were visualized with ChemiDoc MP Imaging System (Bio-Rad), and relative amounts of proteins were quantified by densitometric analysis using Image J software.

2.7. Immunofluorescence analysis

After treatments, the cells were washed twice with PBS, suspended in 2 ml of saline A (8.182 g/l NaCl, 0.372 g/l KCl, 0.336 g/l $NaHCO_3$, and 0.9 g/l glucose, pH 7.4), and incubated for 10 min in 35-mm tissue culture dishes containing an uncoated coverslip. Under these conditions, cells rapidly attach to the coverslip. Subsequently, the cells were fixed for 1 minute with 95 % ethanol and 5 % acetic acid. Following fixation, the cells were washed with PBS. To mitigate non-specific binding, the cells were blocked in PBS containing 2 % bovine serum albumin (BSA) for 30 min at room temperature. Next, the cells were incubated with monoclonal anti-phospho-$p47^{phox}$ or anti-cytochrome c antibodies (diluted 1:100 in PBS containing 2 % BSA) for 18 h at 4 °C. Following antibody incubation, the cells were washed and subsequently incubated for 3 h in the dark with fluorescein isothiocyanate-conjugated secondary antibody (diluted 1:100 in PBS). The cells were finally washed three times with PBS, and fluorescence images were captured with a BX-51 microscope (Olympus, Milan, Italy) equipped with a SPOT-RT camera unit (Diagnostic Instruments, Delta Sistemi, Rome, Italy) using an Olympus LCAch 40 x/0.55 objective lens. The excitation and emission wavelengths were 488 and 525 nm, with a 5-nm slit width for both emission and excitation. Images were acquired digitally and processed at the single-cell level with ImageJ software. Specifically, in the experiments assessing the mitochondrial loss of cytochrome c, the relative numbers of cells exhibiting a punctate fluorescence (indicative of its mitochondrial localization) and diffused fluorescence (suggestive of its mitochondrial loss) were counted. At least 100 cells were analyzed in each experiment to calculate the percentage of cells demonstrating a diffused fluorescence indicative of MPT-dependent mitochondrial loss of cytochrome c.

2.8. NAO fluorescence assay

The cells were supplemented with 10 μM NAO 30 min before the end of the treatments, washed three times with PBS, and subsequently analyzed with the fluorescence microscope. The resulting images were acquired and processed at the single-cell level with ImageJ software. The excitation and emission wavelengths were 488 and 525 nm with a 5-nm slit width for both emission and excitation. Mean fluorescence values were determined by averaging the fluorescence values of at least 100 cells/treatment condition/experiment.

2.9. Measurement of mitochondrial membrane potential

Cells were supplemented to 500 μM MitoTracker red CMXRos for 30 min prior to the end of the treatments. The cells were washed three times, and the fluorescence images were taken and processed as described above. The excitation and emission wavelengths were 545 and 610 nm, with a 5 nm slit width for both emission and excitation. Mean fluorescence values were determined by averaging the fluorescence values of at least 100 cells/treatment condition/experiment.

2.10. Fluorogenic caspase 3 assays

Following the treatments, the cells were lysed with RIPA buffer containing the additions indicated above, pH 7.5. Subsequently, 15 μg of proteins for well were loaded in a 96-well plate with caspase 3 buffer (Hepes 100 mM, Sucrose 10 %, Chaps 0.1 %, EDTA 1 mM, pH 7.5) and caspase 3 substrate (Ac-DEVD- aminomethylcoumarin, 0.4 mM). Caspase 3-like activity was determined fluorometrically in SPECTRA Fluor Plus Microplate Reader Tecan (excitation at 360 nm and emission at 465 nm) by quantifying the release of aminomethylcoumarin from cleaved caspase 3 substrate.

2.11. Analysis of apoptosis with the Hoechst 33342 and comet assays

Apoptotic cells were detected using Hoechst 33342, a blue-fluorescent, DNA-specific dye that selectively stains condensed chromatin, making it a widely used tool in fluorescence microscopy [44,45]. Cells were treated for 15 min with 10 μM Hoechst 33342 and

immediately washed three times with PBS. Fluorescence images were next taken and processed as described above. The relative numbers of cells presenting evidence of chromatin condensation or fragmentation (apoptotic cells) and cells with homogeneously stained nuclei (viable cells) were then counted. The excitation and emission wavelengths were 350 and 420 nm, with a 5 nm slit width for both emission and excitation. The % of Hoechst positive cells was determined by calculating at least 400 cells/treatment condition/experiment.

Apoptotic DNA fragmentation in individual cells was also detected with the comet assay [46]. After treatments, the cells were resuspended at 2.0×10^4 cells/100 µl in 1.0 % low-melting agarose in PBS containing 5 mM ethylenediaminetetraacetic acid (EDTA) and immediately pipetted into agarose-coated slides. The slides were immersed in ice-cold lysing solution (2.5 M NaCl, 100 mM EDTA, 10 mM Tris, 1 % sarkosyl, 5 % dimethyl sulfoxide, and 1 % Triton X-100, pH 10.0) for 60 min. Next, the slides were placed on an electrophoresis tray with an alkaline buffer (300 mM NaOH and 1 mM EDTA) and left for 20 min to allow the DNA to unwind. Electrophoresis was then performed at 300 mA for 20 min in the same alkaline buffer maintained at 14 °C. The slides were subsequently washed and stained for 5 min with 10 µg/ml ethidium bromide. The DNA was visualized by fluorescence microscopy. Mean fluorescence values were determined by averaging the fluorescence values of at least 50 cells/treatment condition/experiment.

2.12. Alkaline-halo assay

DNA single-strand breakage was determined using the alkaline-halo assay developed in our laboratory [47]. DNA damage was quantified by calculating the nuclear spreading factor value, representing the ratio between the area of the halo (obtained by subtracting the area of the nucleus from the total area, nucleus + halo) and that of the nucleus, from 50 to 75 randomly selected cells/experiment/treatment condition. Results are expressed as relative nuclear spreading factor values calculated by subtracting the nuclear spreading factor values of control cells from those of treated cells.

2.13. Measurement of non-protein thiols and GSH content

The cells were washed three times with PBS and the resulting pellets were suspended in (50 µl/10^6 cells) lysis buffer (0.1 % Triton X-100, 0.1 M Na_2HPO_4, 5 mM EDTA, pH 7.5), vortexed and kept for 10 min on an ice bath. Thereafter, (15 µl/10^6 cells) 0.1 N HCl and (140 µl/10^6 cells) precipitating solution (0.2 M glacial meta-phosphoric acid, 5 mM sodium EDTA, 5 M NaCl) were added to the samples. After centrifugation for 10 min at 13,000 x g, the supernatants were collected and kept at −20 °C for the subsequent HPLC and spectrophotometric analyses. The pellets were resuspended in 0.1 N NaOH for protein assay.

GSH levels were evaluated as reported in ref [48]. Just before analysis, 60 µl of the acid extracts were supplemented with 15 µl of 0.3 M Na_2HPO_4 and 15 µl of 5,5-dithiobis (2-nitrobenzoic acid) solution (20 mg in 100 ml of 1 % w/v sodium citrate). The mixture was vortexed for 1 min at room temperature, filtered through 0.22 µm pore micro-filters and analysed for the GSH content by an HPLC assay [49], using a 15 cm× 4.6 mm, 5 µm Supelco Discovery® C18 column (Supelco, Bellefonte, PA). The UV absorption was detected at 330 nm. The injection volume was 20 µl. The retention time of GSH was approximately 17.5 min.

Non-protein thiols (NPSH) content was determined in the acid extracts spectrophotometrically at 412 nm, using 5,5-dithiobis (2-nitrobenzoic acid) ($\varepsilon 412 = 13{,}600\ M^{-1}\ cm^{-1}$), as described in ref [50].

2.14. Enzyme activity assays

The cells (5×10^6) were washed three times with PBS and the resulting pellets were suspended in (50 µl/10^6 cells) lysis buffer (3 mM phosphate buffer pH 7.4; 5 mM glucose; 3 mM KF; 3 mM 2-mercaptoethanol; 1 mM dithiothreitol; 0,5 % Triton X-100), vortexed and kept for 10 min on an ice bath. Samples were sonicated (3 ×10 sec pulse, 100 W), centrifuged (10,000 × g for 10 min at 4°C),

and the activities of catalase and glutathione peroxidase (GPx) as well as the concentration of proteins were measured in the supernatants.

GPx activity was determined at 340 nm, as detailed in ref [50]. The reaction mixture contained 1 M Tris HCl; 5 mM EDTA pH 8; 0.1 M GSH; 10 U /ml glutathione reductase (Sigma G3664); 2 mM NADPH; 7 mM tert-butyl hydroperoxide. One unit of GPx activity is defined as the amount of enzyme catalyzing the production of 1 µmol of NADPH/min.

Catalase activity was determined by measuring the rate of H_2O_2 decomposition at 230 nm [50]. The reaction mixture contained 1 M Tris HCl/5 mM EDTA pH 8, and 10 mM H_2O_2. One unit of catalase activity is defined as the amount of enzyme catalyzing the decomposition of 1 µmol of H_2O_2/min.

2.15. Statistical analysis

All the results were reported as mean ± standard deviation (SD) and calculated from at least three distinct experiments. GraphPad Prism software version 9.0.0 (GraphPad Software Inc., La Jolla, CA) was used to create graphs and perform data analyses. Statistical differences were analyzed by or one-way ANOVA followed by Tukey's test to compare every mean with every other mean or Dunnett's test to compare every mean to a control mean. The P value of < 0.05 indicated statistical significance.

3. Results

3.1. Susceptibility of NB4, U937 and THP-1 cells to ATO induced mitochondrial ROS formation

NB4, U937 and THP-1 cells were exposed for 6 h to 0.5–1.0 µM ATO and then processed for the analysis of the fluorescence observed with MitoSOX red, which only detects mito$O_2^{\cdot-}$ [43], or DHR, that reveals the presence of different types of ROS in the cytosol, including diffusible H_2O_2 produced in the mitochondria [51]. In these experiments we also used rotenone (0.5 µM), an inhibitor of complex I [52], under conditions in which it effectively prevents the entry of electrons in complex I, thereby abolishing oxygen consumption (not shown). The rotenone-sensitive fraction of the fluorescence responses observed with MitoSOX red and DHR is therefore indicative of ROS formation in the mitochondrial respiratory chain.

ATO induced significant MitoSOX red (Fig. 1A) and DHR (Fig. 1B) fluorescence signals in NB4 cells, with hardly any effect detected in U937 or THP-1 cells. Rotenone completely or partially suppressed the ROS response of NB4 cells respectively detected with MitoSOX red or DHR.

We next performed experiments in which ATO was replaced with $NaAsO_2$, which, at low micromolar ($\leq$ 2.5 µM) concentrations, promotes the exclusive formation of mito$O_2^{\cdot-}$ [53]. The 6 h exposure to 1–2.5 µM $NaAsO_2$ triggered similar MitoSOX red (Fig. 1C) and DHR (Fig. 1D) fluorescence responses in NB4, U937 and THP-1 cells, in all these circumstances invariably suppressed by rotenone.

We finally addressed the issue of whether higher ATO concentrations can induce the formation of mitochondrial ROS in resistant cells. Exposure of U937 cells to 5 µM ATO triggered significant MitoSOX red (Fig. 1E) and DHR (Fig. 1F) fluorescence signals, respectively suppressed and only partially inhibited by rotenone.

3.2. Susceptibility of NB4, U937 and THP-1 cells to ATO induced NOX 2 activation

NB4, U937 and THP-1 cells were exposed for 6 h to 0.5 and 1 µM ATO and then analyzed for NOX 2 activity. Western blot (Fig. 2A-C) and immunocytochemical (Fig. 2D-F) assays provided clear evidence of

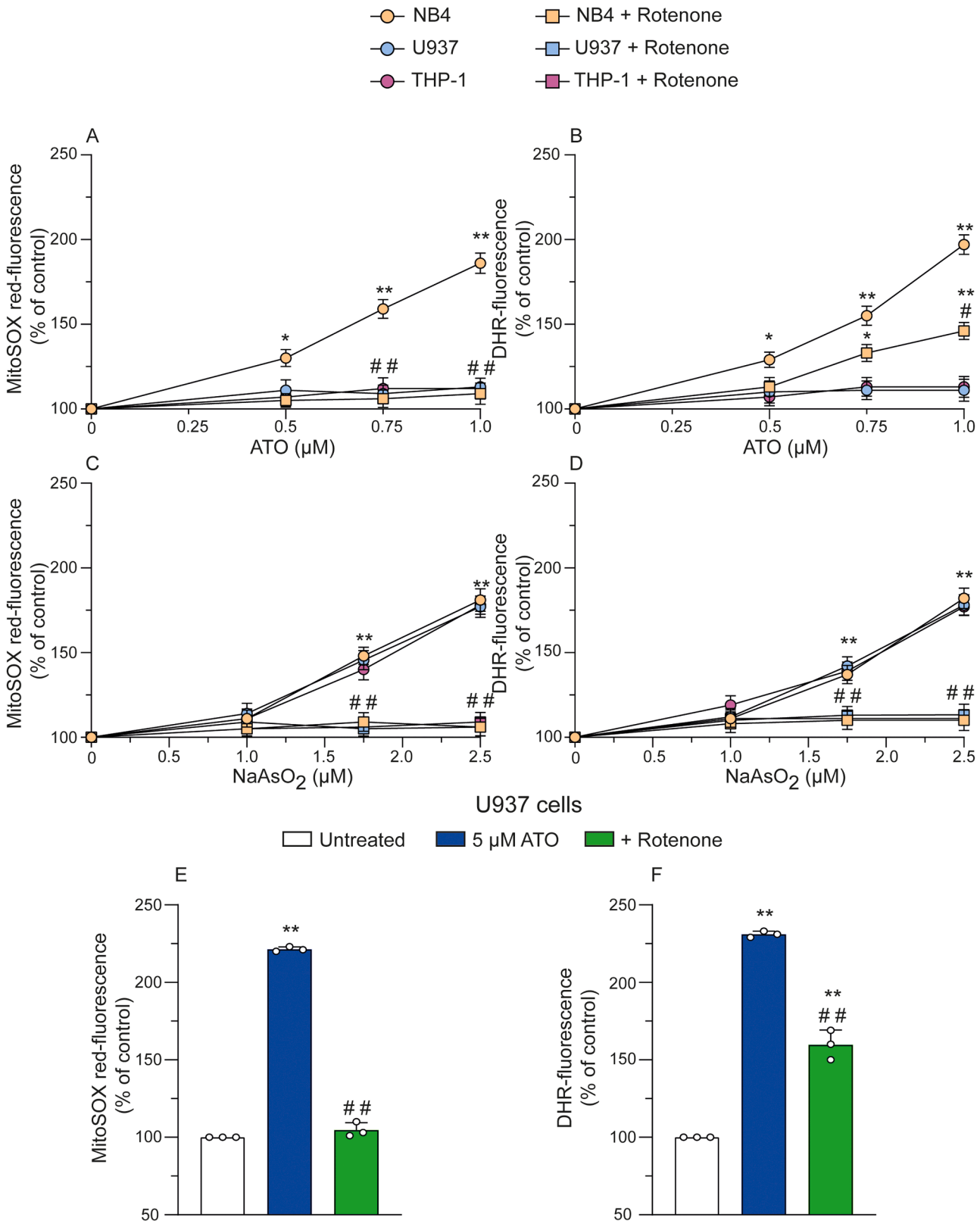

Fig. 1. Susceptibility of NB4, U937 and THP-1 cells to ATO induced mitochondrial ROS formation.NB4, U937 or THP-1 (A-D) cells were pretreated for 5 min with the vehicle or 0.5 μM rotenone and incubated for 6 h with increasing concentrations of ATO (A, B), or $NaAsO_2$ (C, D). After treatments, the cells were analyzed for MitoSOX red- (A, C) or DHR- (B, D) fluorescence, as detailed in the Materials and Methods section. In other experiments, U937 were incubated for 6 h with 5 μM ATO, alone or associated with rotenone, and analyzed for MitoSOX red- (E) or DHR- (F) fluorescence. Results represent the means ± SD calculated from three separate experiments. *P < 0.05, * *P < 0.01, compared with untreated cells. #P 0.05, ##P < 0.01 compared with ATO or $NaAsO_2$ treated cells (one-way ANOVA followed by Tukey test).

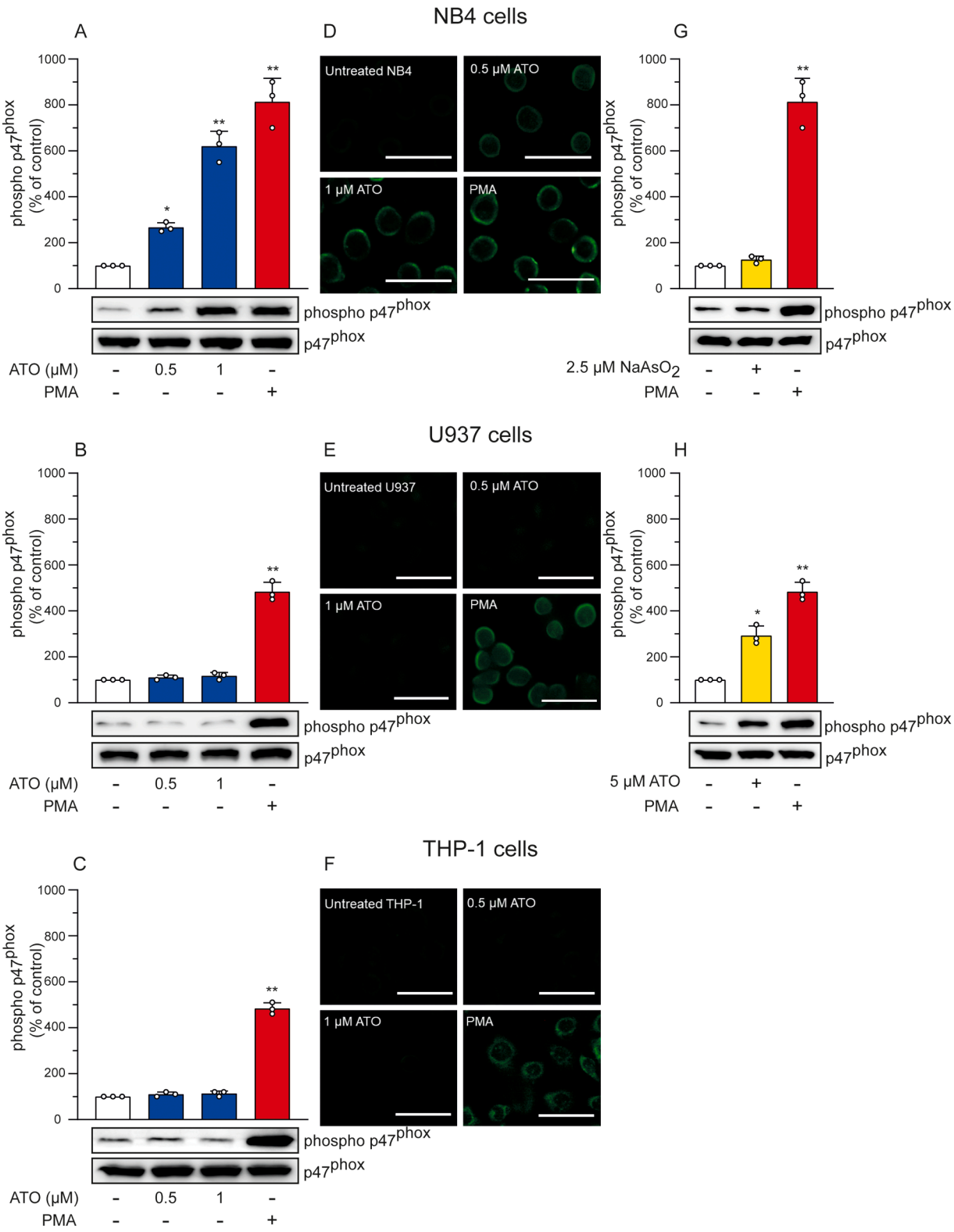

Fig. 2. Clinically relevant concentrations of ATO stimulate phosphorylation of phospho p47^{phox} in NB4 but not in U937 or THP-1 cells.NB4 (A, D), U937 (B, E) or THP-1 (C, F) cells were incubated for 6 h with 0.5 or 1 μM ATO. In other experiments, NB4 (G) or U937 (H) cells were treated for 6 h with 2.5 $NaAsO_2$ or 5 μM ATO, respectively. PMA (0.162 μM, 15 min) was used as a positive control. After treatments, the cells were analyzed for phospho p47^{phox} expression (A-H). The blot, representative of three separate experiments, was re-probed for p47^{phox}. Representative micrographs providing immunocytochemical evidence of p47^{phox} phosphorylation are also reported in panel D (NB4 cells), E (U937 cells) and F (THP-1 cells). After treatments, the cells were fixed and processed as detailed in Material and Methods. Scale bar represents 20 μm. Results represent the means ± SD calculated from three separate experiments. *P < 0.05, * *P < 0.01, compared with untreated cells (one-way ANOVA followed by Dunnett's test).

increased $p47^{phox}$ phosphorylation in NB4 cells, with hardly any effect detected in U937 and THP-1 cells. The effects of ATO in NB4 cells were concentration dependent. Importantly, PMA, an agent directly stimulating NOX 2 activity [54], significantly increased $p47^{phox}$ phosphorylation in NB4 cells and, to a lower extent, in U937 and THP-1 cells (Fig. 2A-F).

We also performed Western blot studies in NB4 cells exposed for 6 h to 2.5 μM $NaAsO_2$, which failed to enhance $p47^{phox}$ phosphorylation, instead observed with PMA (Fig. 2G), thereby further supporting the notion that, under these conditions, this arsenic compound promotes the exclusive formation of mito$O_2^{\cdot-}$.

We finally asked the question of whether high ATO concentrations activate NOX 2 in resistant U937 cells. As shown in Fig. 2H, a 6 h exposure to 5 μM ATO increased $p47^{phox}$ phosphorylation also in these cells, an observation in keeping with the previous data (Fig. 1F) indicating that rotenone only partially reduces the resulting DHR fluorescence signal. PMA was used as an internal positive control.

3.3. Pharmacological inhibition of NOX 2 suppresses mitochondrial ROS formation induced by ATO in NB4 cells

We investigated whether $O_2^{\cdot-}$ formation in mitochondria and *via* NOX 2 activation are mechanistically connected. Our previous observation that, in NB4 cells, rotenone completely suppresses mito$O_2^{\cdot-}$ formation (Fig. 1A), but nevertheless leaves some residual DHR fluorescence (Fig. 1B), suggests that mito$O_2^{\cdot-}$ emission is not upstream to NOX 2. A similar observation was also made in experiments using high ATO concentrations in resistant cells (Fig. 1F).

To test the possibility of an opposite regulation, i.e., that NOX 2 lies upstream to mito$O_2^{\cdot-}$ formation, we performed experiments using two different inhibitors of this enzyme, apocynin and DPI [32]. We initially demonstrated that both inhibitors blunt $p47^{phox}$ phosphorylation (Fig. 3A) and the DHR fluorescence response (Fig. 3B) induced by PMA. Next, we showed that apocynin, or DPI, suppress $p47^{phox}$ phosphorylation (Fig. 3C) as well as the associated MitoSOX red (Fig. 3D) and DHR (Fig. 3E) fluorescence responses induced by 1 μM ATO.

These results are consistent with the possibility that NOX 2 activation is upstream to, and causally connected with mito$O_2^{\cdot-}$ formation. On the other hand, these results could also be explained by the reported antioxidant effects of apocynin and DPI [32].

To address this issue, we performed experiments in which NB4 cells were exposed for 6 h to 2.5 μM $NaAsO_2$. The resulting MitoSOX (Fig. 3F) and DHR (Fig. 3G) fluorescence responses were blunted by rotenone, as previously shown (Fig. 1C and D), and were instead insensitive to apocynin or DPI. Thus, these inhibitors fail to scavenge mito$O_2^{\cdot-}$ and H_2O_2 generated by 2.5 μM $NaAsO_2$ under conditions characterized by the absence of NOX 2 activation.

In other experiments, we employed a higher concentration of $NaAsO_2$ (5 μM) causing apocynin, or DPI, sensitive, and rotenone insensitive, $p47^{phox}$ phosphorylation (Fig. 3H). Interestingly, $NaAsO_2$ promoted a MitoSOX red fluorescence response sensitive to rotenone and insensitive to apocynin or DPI (Fig. 3I). Finally, the DHR fluorescence response detected under identical conditions was partially inhibited by rotenone and, to a somewhat lower extent, by apocynin, or DPI (Fig. 3L).

3.4. ATO fails to promote mitochondrial ROS formation in NB4 cells with downregulated NOX 2 expression

To provide more evidence supporting the upstream role of NOX 2 activation in the triggering of ATO induced mito$O_2^{\cdot-}$ emission, we used a strategy based on downregulation of NOX 2 expression. NB4 cells were therefore transfected with $p47^{phox}$-specific siRNA, which caused an about 50 % inhibition of $p47^{phox}$ protein expression, compared to non-transfected cells, or cells transfected with the scrambled siRNA (Fig. 4A). Reduced expression of NOX 2 was associated with markedly reduced PMA-dependent DHR fluorescence, which, as previously observed in non-transfected cells (Fig. 3B), was in both scrambled and specific $p47^{phox}$ siRNA transfected cells invariably sensitive to both DPI and apocynin (Fig. 4B). We then showed that 1 μM ATO induces a low, rotenone insensitive and apocynin, or DPI, sensitive fluorescence signal in cells transfected with the $p47^{phox}$ specific siRNA (Fig. 4C). These results are therefore consistent with the proposed paradigm of mito$O_2^{\cdot-}$ formation downstream to NOX 2 activation. The results obtained in cells transfected with the scrambled siRNA, were in line with those from non-transfected cells (Figs. 1B and 3E) and provided clear evidence of significant NOX 2 activation, which, based on inhibitor studies, is upstream to mito$O_2^{\cdot-}$ formation.

Consistently, ATO failed to promote a statistically significant MitoSOX red fluorescence response in cells transfected with the $p47^{phox}$ siRNA (Fig. 4D), whereas the results obtained with cells transfected with the scrambled siRNA were like those from non-transfected cells (Figs. 1A and 3F).

3.5. Low mitochondrial ROS formation induced by ATO in resistant cells is due to poor activation of NOX 2

We investigated whether the resistance phenotype in AML cells could be overcome by enhancing NOX 2 activity, which is only weakly stimulated by 1 μM ATO, through the addition of PMA. This approach seems viable, as PMA alone is known to induce NOX 2-dependent ROS formation without triggering concomitant mito$O_2^{\cdot-}$ emission under basal conditions [43]. Thus, the central question was whether the PMA-induced phosphorylation of p47phox enhances mito$O_2^{\cdot-}$ emission in AML cells treated with ATO.

U937 and THP-1 cells were therefore exposed for 6 h to 0.5 or 1 μM ATO, or to PMA, and finally processed for MitoSOX red fluorescence analysis. As indicated in Fig. 5, none of these treatments elicited mito$O_2^{\cdot-}$ formation in U937 (A) and THP-1 (B) cells, as expected. The mitochondrial ROS response was instead dramatically and dose-dependently induced under conditions in which ATO and PMA were used in combination. A second important finding from these experiments was that the MitoSOX red fluorescence response is in both cell lines suppressed by rotenone as well as by apocynin or DPI.

The results obtained using $p47^{phox}$ siRNA transfected NB4 cells (Fig. 5C) were in line with those discussed above, although combined treatment with ATO and PMA produced a much lower fluorescence response than that generated in U937 and THP-1 cells, most likely due to their downregulated NOX 2 expression.

3.6. Clinically relevant concentrations of ATO promote mitochondrial permeability transition-dependent apoptosis in susceptible NB4 cells

The formation of mito$O_2^{\cdot-}$ is expected to promote mitochondrial dysfunction. We found that the 6 h exposure of NB4 cells to 1 μM ATO is associated with the induction of a significant NAO fluorescence response, indicative of cardiolipin oxidation ([55], Fig. 6A). This response was blunted by both rotenone and apocynin.

Additional studies provided evidence for a reduction in mitochondrial membrane potential at 9 h (Fig. 6B) (otherwise not observed at 6 h, Fig. S1A), an event prevented by rotenone, apocynin as well as 0.5 μM CsA, a MPT inhibitor [56]. At the same time point, we also obtained evidence for the mitochondrial loss of cytochrome c associated with its concomitant appearance in the cytosol (see methods section). This event was also sensitive to rotenone, apocynin or CsA (Fig. 6C).

In other experiments, we found no evidence of caspase 3 activation (Fig. S1B), or apoptotic DNA fragmentation (Fig. S1C and D) at 9 h. These responses were instead clearly detected at 14 h and were in both circumstances sensitive to CsA, rotenone or apocynin (Fig. 6D, E and F).

We performed all the above experiments also in cells transfected with the scrambled siRNA obtaining results in line with those from non-transfected NB4 cells. In cells transfected with the $p47^{phox}$ specific

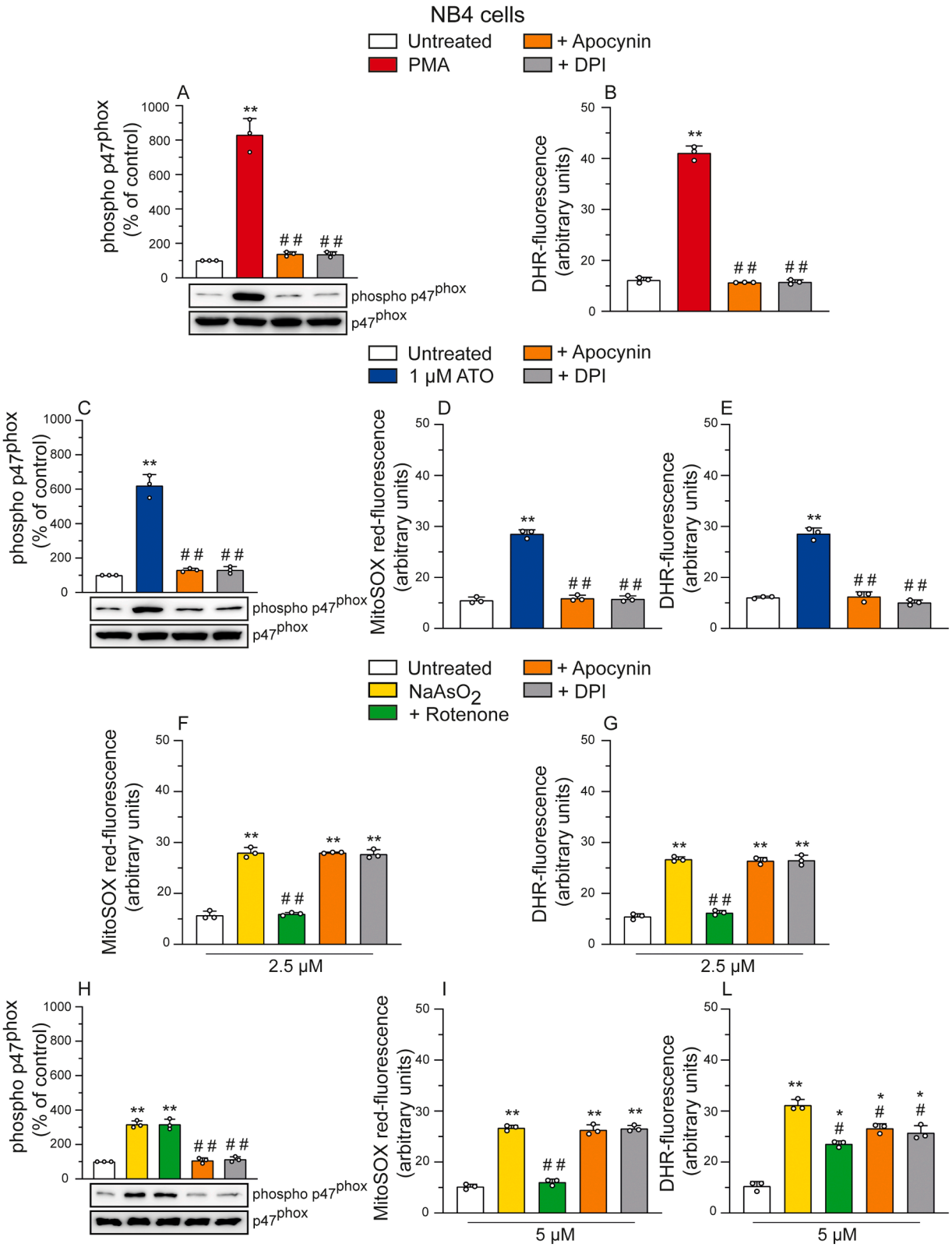

Fig. 3. Pharmacological inhibition of NOX 2 activity suppresses mitochondrial ROS formation induced by ATO in NB4 cells.NB4 cells were pretreated for 5 min with the vehicle, 10 μM apocynin, or 1 μM DPI, and exposed for 15 min to 0.162 μM PMA. After treatments, the cells were analyzed for phospho $p47^{phox}$ expression (A) or DHR-fluorescence (B). NB4 cells pretreated as indicated above or with rotenone, were exposed for 6 h to 1 μM ATO. After treatments, the cells were analyzed for phospho $p47^{phox}$ expression (C), MitoSOX red- (D) or DHR- (E) fluorescence. In other experiments, the cells were pretreated with the vehicle, rotenone, apocynin or DPI, incubated for 6 h with 2.5 (F, G) or 5 μM (H-L) $NaAsO_2$ and finally analyzed for MitoSOX red- (F, I) and DHR- (G, L) fluorescence, or for phospho $p47^{phox}$ expression (H). The relative band intensity of phospho $p47^{phox}$ is depicted in the top bar chart. $p47^{phox}$ was accounted for loading control. Results represent the means ± SD calculated from three separate experiments. *P < 0.05, * *P < 0.01, compared with untreated cells. #P < 0.05, ##P < 0.01 compared with ATO or NaAsO2 treated cells (one-way ANOVA followed by Tukey test).

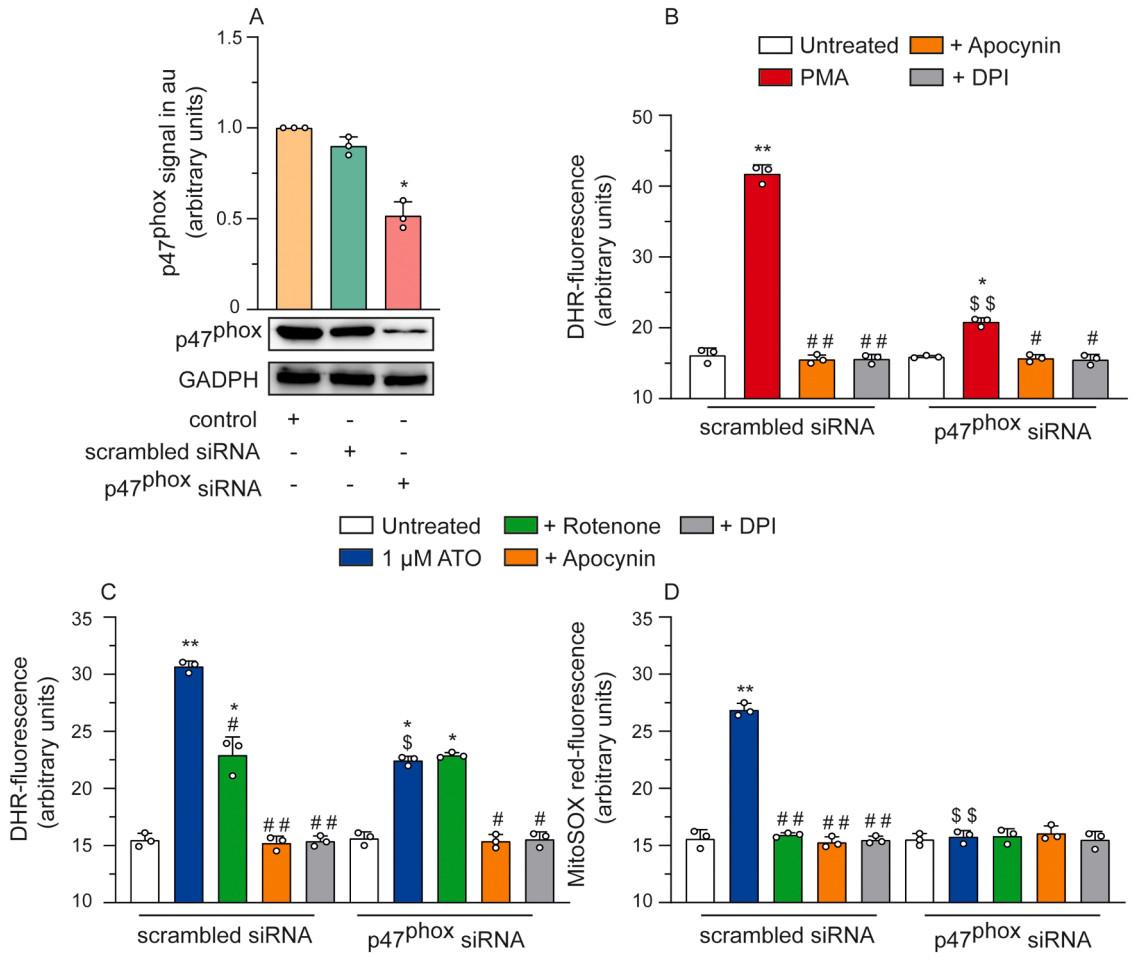

Fig. 4. ATO fails to promote mitochondrial ROS formation in NB4 cells with downregulated p47^{phox} expression.NB4 control cells, transfected with scrambled or p47^{phox} siRNA, were lysed and analyzed by Western blotting 48 h post-transfection using anti-p47^{phox} antibody. The relative band intensity of p47^{phox} is depicted in the top bar chart (A). GADPH was accounted for loading control. Results represent the means ± SD calculated from three separate experiments. *P < 0.05, compared with control cells (one-way ANOVA followed by Dunnett's test).Cells transfected with scrambled or p47^{phox} specific siRNA were pretreated for 5 min with the vehicle, apocynin, or DPI and exposed for either 15 min to PMA (B) or 6 h to 1 μM ATO (C, D). In some experiments, rotenone was added to the cultures 5 min before ATO. After treatments, the cells were analyzed for DHR- (B, C) or MitoSOX red- (D) fluorescence. Results represent the means ± SD calculated from three separate experiments. *P < 0.05, * *P < 0.01, compared with untreated cells. #P < 0.05, ##P < 0.01 compared with ATO treated cells. $P < 0.05, $$P < 0.01 compared with treated scrambled siRNA cells (ANOVA followed by Tukey test).

siRNA, exposure to ATO failed to promote a statistically significant NAO fluorescence (Fig. 6A). In addition, there was no evidence for a decline in mitochondrial membrane potential (Fig. 6B) and mitochondrial loss of cytochrome c (Fig. 6C) at 9 h. Lastly, these cells were resistant to the effects of ATO also in terms of caspase 3 activation (Fig. 6D) and apoptotic DNA fragmentation detected at 14 h (Fig. 6E and F).

3.7. Significant differences in susceptibility to ATO-induced apoptosis and comparable antioxidant defenses between APL and AML cell lines

We conducted experiments in which three cell types were treated with increasing concentrations of ATO for 14 hours. Apoptotic cells, identified by condensed or fragmented chromatin, were quantified using the Hoechst assay (Fig. 7A). To complement this, we employed the comet assay as an additional method to assess apoptosis (Fig. 7B). This technique detects DNA fragmentation characteristic of apoptosis, where the fragments migrate under an electric field, producing a distinctive "comet tail" when viewed under a microscope.

The results from the two assays were nearly identical, showing that clinically relevant concentrations of ATO did not induce toxicity in AML cell lines, instead detected at concentrations $\geq$ 5 μM. Different results were obtained with NB4 cells, which responded to ATO with a dose dependent apoptotic DNA fragmentation, clearly detected even at clinically relevant concentrations of the drug.

We next investigated the redox status of the APL and AML cell lines, previously suggested to partially account for their differing susceptibilities to ATO [27,30,40]. As illustrated in Fig. 7, NB4, U937 and THP-1 cells exhibited comparable levels of cellular NPSH (C), GSH (D), catalase (E) and GPx (F). The efficiencies of their antioxidant systems were indirectly evaluated, using reagent H_2O_2. As indicated in Fig. 7G, a 30 min exposure to increasing concentrations of the oxidant resulted in a comparable, dose-dependent accumulation of DNA single-strand breaks in the three cell lines.

In control experiments, treatment of U937 cells with 10 mM ATZ (6 h) reduced catalase activity by 70 % (data non shown), and significantly amplified the DNA damaging response evoked by a 30 min exposure to 50 μM H_2O_2 (Fig. S2).

In additional experiments, we investigated ATO's ability to induce the expression of Nrf2 and its downstream target, NQO1, in NB4, U937, and THP-1 cells. Notably, treatment with 1 μM ATO significantly increased the expression of both Nrf2 (Fig. 7H) and NQO1 (Fig. 7I) in NB4 cells, while U937 and THP-1 cells showed minimal response. Furthermore, neither rotenone nor apocynin influenced the Nrf2 and NQO1 upregulation induced by ATO in NB4 cells.

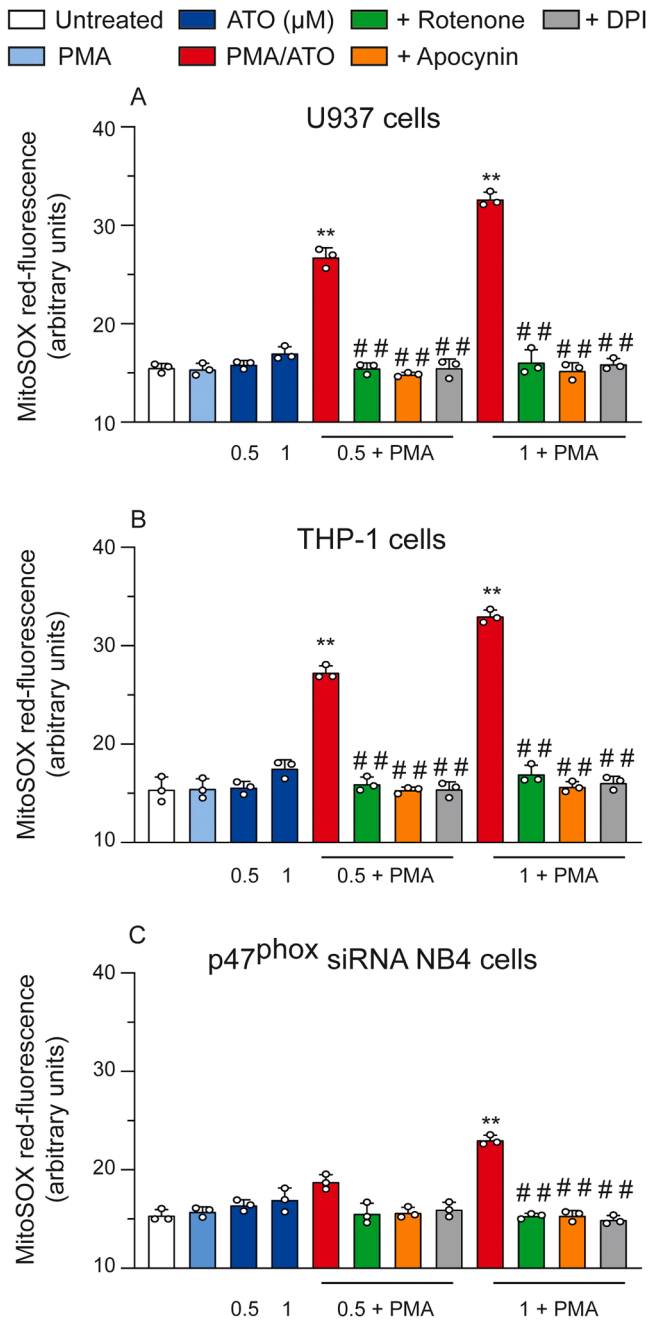

Fig. 5. Low mitochondrial ROS formation induced by ATO in resistant cells is due to poor activation of NOX 2.U937 (A), THP-1 (B) or $p47^{phox}$ siRNA transfected NB4 (C) cells were pretreated for 5 min with the vehicle, rotenone, apocynin or DPI and incubated for 6 h with 0.5 or 1 μM ATO alone or associated PMA. After treatments, the cells were analyzed for MitoSOX red fluorescence. Results represent the means ± SD calculated from three separate experiments. * $^*P < 0.01$, compared with untreated cells. ##$P < 0.01$ compared with ATO/PMA treated cells (ANOVA followed by Tukey test).

3.8. PMA rescues ATO resistance to MPT-dependent apoptosis in AML cell lines

Having previously demonstrated that mito$O_2^{\cdot-}$ production is enhanced when NOX 2 activity is directly stimulated with PMA (Fig. 5A, B), we investigated whether these conditions might also trigger delayed apoptosis in otherwise resistant cells. U937 and THP-1 cells were treated for 9 hours with 1 μM ATO, PMA, or a combination of both, followed by an assessment of mitochondrial membrane potential. As expected, neither ATO nor PMA alone affected the mitochondrial membrane potential (Fig. 8A, D). However, combined treatment with ATO and PMA induced a significant decline in mitochondrial membrane potential, sensitive to rotenone, apocynin, and CsA.

At 14 h, a time at which neither ATO nor PMA alone caused detectable chromatin fragmentation or condensation, combined treatment clearly induced apoptotic DNA fragmentation in U937 (Fig. 8B, C) and THP-1 (Fig. 8E, F) cells. This apoptotic effect was suppressed by rotenone, apocynin, or CsA. Apoptotic DNA fragmentation was confirmed using both the Hoechst assay (Fig. 8B, E) and the comet assay (Fig. 8C, F)

4. Discussion

Clinically relevant concentrations of ATO induce apoptosis in APL cells through multiple mechanisms, in particular by promoting the formation of ROS *via* NOX 2 activation and in the mitochondrial respiratory chain [23,29,41]. The susceptibility of these cells to ATO, while still poorly understood, accounts for the efficacy of the arsenic compound in targeting APL and concomitantly sparing normal hemopoietic cells [19,27,29]. Furthermore, poorly defined are also the reasons of the resistance of other hematological tumors, e.g., AML, to ATO induced ROS formation and toxicity.

To elucidate the mechanisms underlying the differing susceptibilities of APL and AML cells, this study focused on the early events of ROS formation, both within the mitochondria and through NOX 2 activation, triggered by clinically relevant concentrations of ATO.

We initially recapitulated the findings from other reports [19,27,29] and showed that 0.5–1 μM ATO promotes mito$O_2^{\cdot-}$ formation in NB4 cells, in the absence of detectable effects in U937 and THP-1 cells, which were observed only at higher, clinically irrelevant concentrations. Interestingly, however, the three cell types responded to a low concentration of $NaAsO_2$ with the same rate of mito$O_2^{\cdot-}$ emission. This implies that the two arsenic compounds mediate mitochondrial ROS formation *via* different mechanisms and that the mitochondrial machinery responsible for $O_2^{\cdot-}$ formation is equally efficient in the three cell types.

Next, we demonstrated that ATO induces mito$O_2^{\cdot-}$ emission concomitantly with a second mechanism of ROS formation, associated with NOX 2 activation. This was true in the case of NB4 cells treated with $\leq$ 1 μM ATO as well as of U937 cells challenged by a high ATO concentration (5 μM).

While concomitant induction of the two mechanisms of ROS formation can only be circumstantial, the possibility of their crosstalk was nevertheless taken into consideration, since other studies [57–59] have previously demonstrated that, under different conditions, each of the two mechanisms can be upstream, and critically contribute to the positive regulation of the other.

The possibility that mito$O_2^{\cdot-}$ contributes to NOX 2 activation induced by ATO, is however in contrast with the observation that prevention of mitochondrial ROS formation with rotenone fails to impact on $p47^{phox}$ phosphorylation and NOX 2-dependent $O_2^{\cdot-}$ formation. These findings are instead compatible with the possibility that NOX 2 derived $O_2^{\cdot-}$ is required for ATO induced mito$O_2^{\cdot-}$ formation. This second hypothesis is also in keeping with the observation that apocynin and DPI, while completely suppressing both $p47^{phox}$ phosphorylation and ROS formation induced by PMA, caused identical suppressive effects of $p47^{phox}$ phosphorylation as well as of the MitoSOX red and DHR fluorescence responses induced by ATO. Thus, in NB4 cells, pharmacological inhibition of NOX 2 activity leads to suppression of ATO induced mito$O_2^{\cdot-}$ formation.

The possibility of a NOX 2 dependent regulation of mito$O_2^{\cdot-}$ formation induced by ATO in sensitive cells was further explored and implemented with data indicating that the effects mediated by apocynin, or DPI, are not associated with non-specific radical scavenging, and are in fact causally linked to inhibition of NOX 2.

In a first set of experiments performed in NB4 cells, ATO was

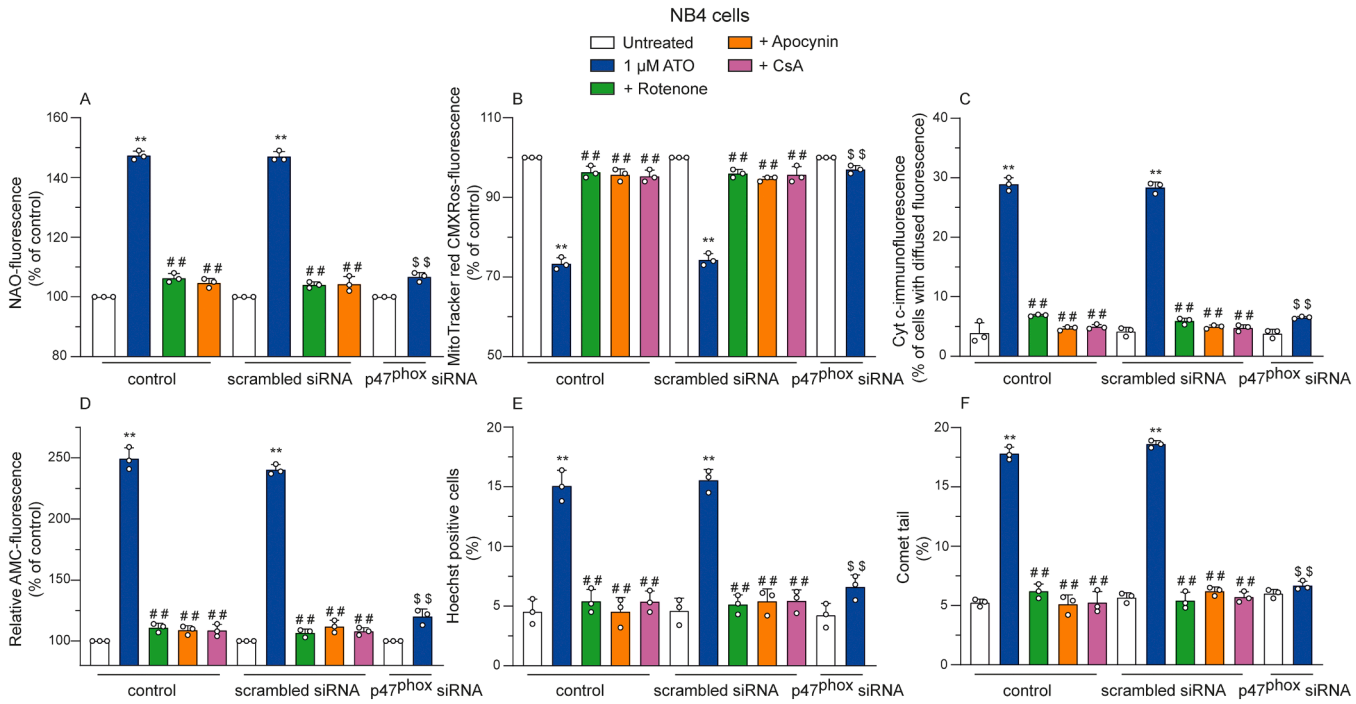

Fig. 6. Clinically relevant concentrations of ATO promote mitochondrial permeability transition-dependent apoptosis in susceptible NB4 cells. NB4 control cells, and NB4 cells previously transfected with scrambled or specific $p47^{phox}$ siRNA, were pretreated for 5 min with the vehicle, rotenone, apocynin or 0.5 μM CsA and incubated for 6 (A), 9 (B, C) or 14 (D, E, F) h with 1 μM ATO. After treatments, the cells were analyzed for NAO-fluorescence (A) MitoTracker red CMXRos-fluorescence (B), cytochrome c (Cyt c) localization (C), caspase 3 activity (D) and apoptotic DNA fragmentation/condensation by both the Hoechst (E) and comet (F) assays. * *P < 0.01, compared with untreated cells. ##P < 0.01 compared with ATO treated cells. $$P < 0.01 compared with ATO treated scrambled siRNA cells (one-way ANOVA followed by Tukey test).

replaced with a concentration of $NaAsO_2$ generating $mitoO_2^{\cdot-}$ in the absence of detectable NOX 2 activation [60,61]. We observed that the fluorescent signal obtained under these conditions with probes specifically detecting mitochondrial and extramitochondrial ROS was suppressed by rotenone and insensitive to both apocynin and DPI. These results indicate that the NOX 2 inhibitors fail to scavenge intramitochondrial $O_2^{\cdot-}$ as well as the H_2O_2 generated upon its dismutation and diffused in the cytosol.

In the second set of experiments, we used a higher concentration of $NaAsO_2$ causing concomitant, albeit independent release of both mitochondrial and NOX 2 derived ROS. Once again, rotenone suppressed the ensuing MitoSOX red fluorescence response, that was instead insensitive to apocynin or DPI. Interestingly, the NOX 2 inhibitors on one side, and rotenone on the other, only partially inhibited the DHR fluorescence signal mediated by the high concentration of $NaAsO_2$. Thus, under conditions associated with the concomitant formation of $O_2^{\cdot-}$ in mitochondria and *via* NOX 2 activation, apocynin and DPI spared the fraction of rotenone sensitive ROS, and hence specifically blunted NOX 2 dependent ROS.

Final important evidence supporting the specificity of the findings obtained in the above inhibitor studies derives from experiments using NB4 cells transfected with $p47^{phox}$ specific siRNA. The DHR fluorescence response induced in these cells by PMA or ATO was lower than that observed in cells transfected with the scrambled siRNA and was in both circumstances suppressed by apocynin or DPI. Importantly, the DHR fluorescence response induced by ATO in cells with downregulated NOX 2 activity was insensitive to rotenone. As a final note, ATO failed to promote detectable MitoSOX red fluorescence in these cells.

Thus, these results collectively provide compelling evidence in support of the notion that $mitoO_2^{\cdot-}$ formation induced by ATO in sensitive cells requires cytosolic ROS generated by upstream NOX 2 activation.

It is well established that $mitoO_2^{\cdot-}$ is readily dismutated within mitochondria by an organelle specific isoform of superoxide dismutase to H_2O_2, which can easily cross the inner and outer mitochondrial membranes [62,63]. Thus, H_2O_2 escaping metabolism can mediate deleterious effects in mitochondria, also associated with the induction of MPT [64,65], as well as in extramitochondrial targets.

The formation of $mitoO_2^{\cdot-}$ in NB4 cells exposed to ATO is expected to trigger a cascade of events culminating in the induction of the mitochondrial pathway of apoptosis [27,28,40].

Consistently, we obtained evidence of cardiolipin oxidation at 6 h. Cardiolipin is primarily located in the mitochondrial inner membrane and is susceptible to oxidative modifications induced by mitochondrial ROS [55], which can impair its function in maintaining mitochondrial membrane integrity [55]. A decline in mitochondrial membrane potential associated with mitochondrial loss of cytochrome c was then detected at 9 h and these events were followed by caspase 3 activation and apoptotic DNA fragmentation at 14 h.

Thus, $mitoO_2^{\cdot-}$ formation induced by ATO is associated with the triggering of the mitochondrial pathway of apoptosis, which was consistently blunted by specifically targeting $mitoO_2^{\cdot-}$ emission with rotenone. In addition, in keeping with the upstream role of NOX 2 in $mitoO_2^{\cdot-}$ formation, the suppressive effects of rotenone were recapitulated by apocynin and downregulation of NOX 2 expression.

We can therefore conclude that the elevated NOX 2 activation mediated by clinically relevant concentrations of ATO in APL cells likely accounts for the high susceptibility of these cells to $mitoO_2^{\cdot-}$ formation and to the ensuing MPT-dependent apoptosis.

As a corollary, resistance of AML cells appears to depend on their low expression/activity of NOX 2, clearly detected in this and other studies [23,29,30]. This issue was addressed in rescue experiments using U937 and THP-1 cells treated with 1 μM ATO, in which the further addition of PMA triggered an elevated formation of $mitoO_2^{\cdot-}$. This is an interesting observation since, under identical conditions, ATO or PMA alone failed to promote detectable effects. Consistent findings were obtained in NB4 cells transfected with $p47^{phox}$ siRNA.

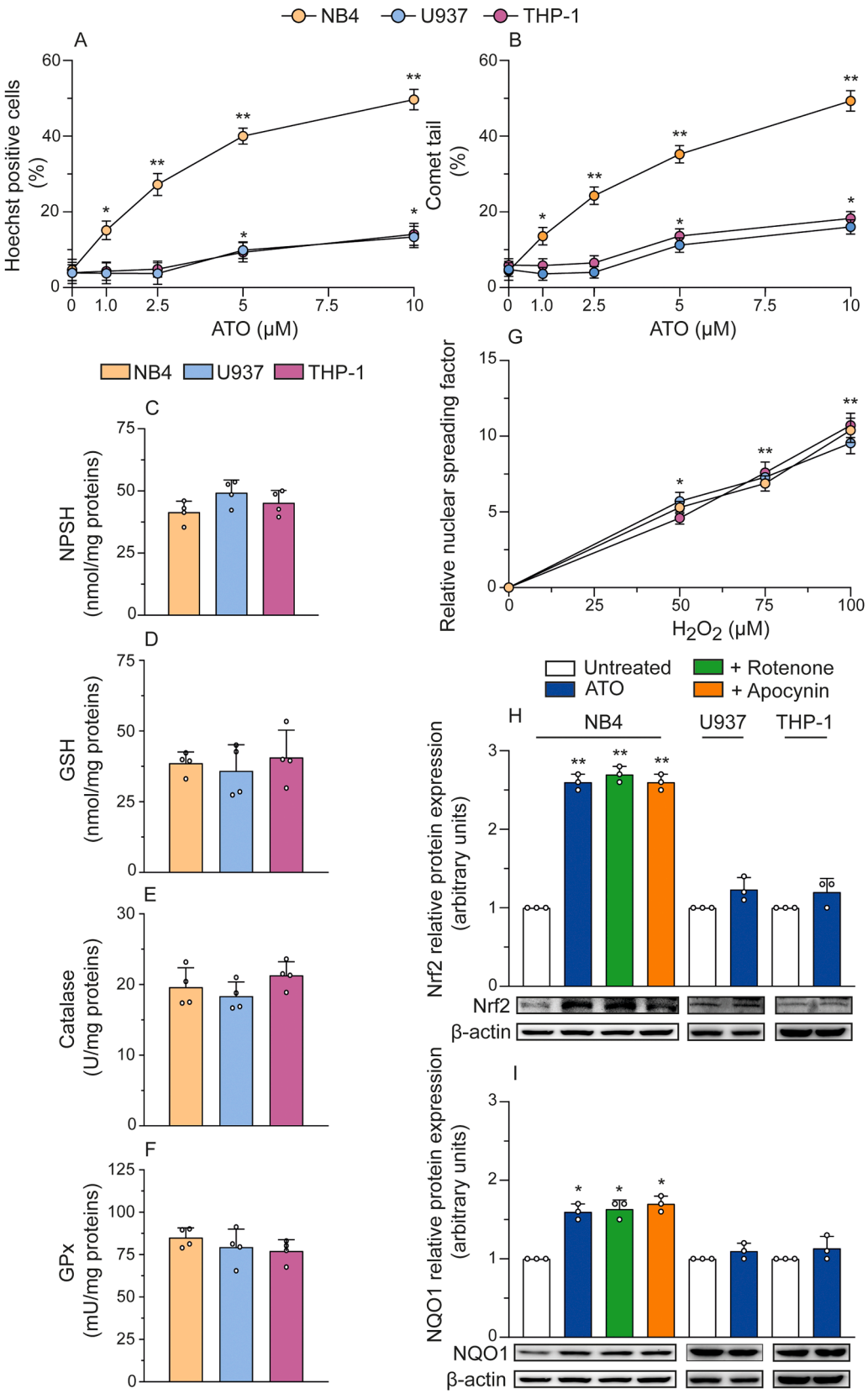

(caption on next page)

Fig. 7. Baseline antioxidant system and Nrf2 antioxidant stress response to ATO in sensitive and resistant cells. NB4, U937 or THP-1 cells were exposed for 14 h to increasing concentrations of ATO and analyzed for apoptotic DNA fragmentation/condensation by the Hoechst (A) and comet (B) assays. NB4, U937 or THP-1 cells were analyzed for NPSH (C) and GSH (D) content, as well as for catalase (E) and GPx (F) activity, as described in Material and Methods. In other experiments, the cells were exposed for 30 min to increasing concentrations of H_2O_2 and analyzed for DNA damage with the alkaline-halo assay (G). NB4, U937 or THP-1 cells were pretreated for 5 min with the vehicle, rotenone or apocynin and exposed for 6 h to 1 μM ATO. After treatments, cells were analyzed for Nrf2 (H) and NQO1 (I) expression. β-actin was accounted for loading control. The results represent the means ± SD calculated from at least three distinct experiments. *P < 0.05, * *P < 0.01, compared with untreated cells (one-way ANOVA followed by Dunnett's test).

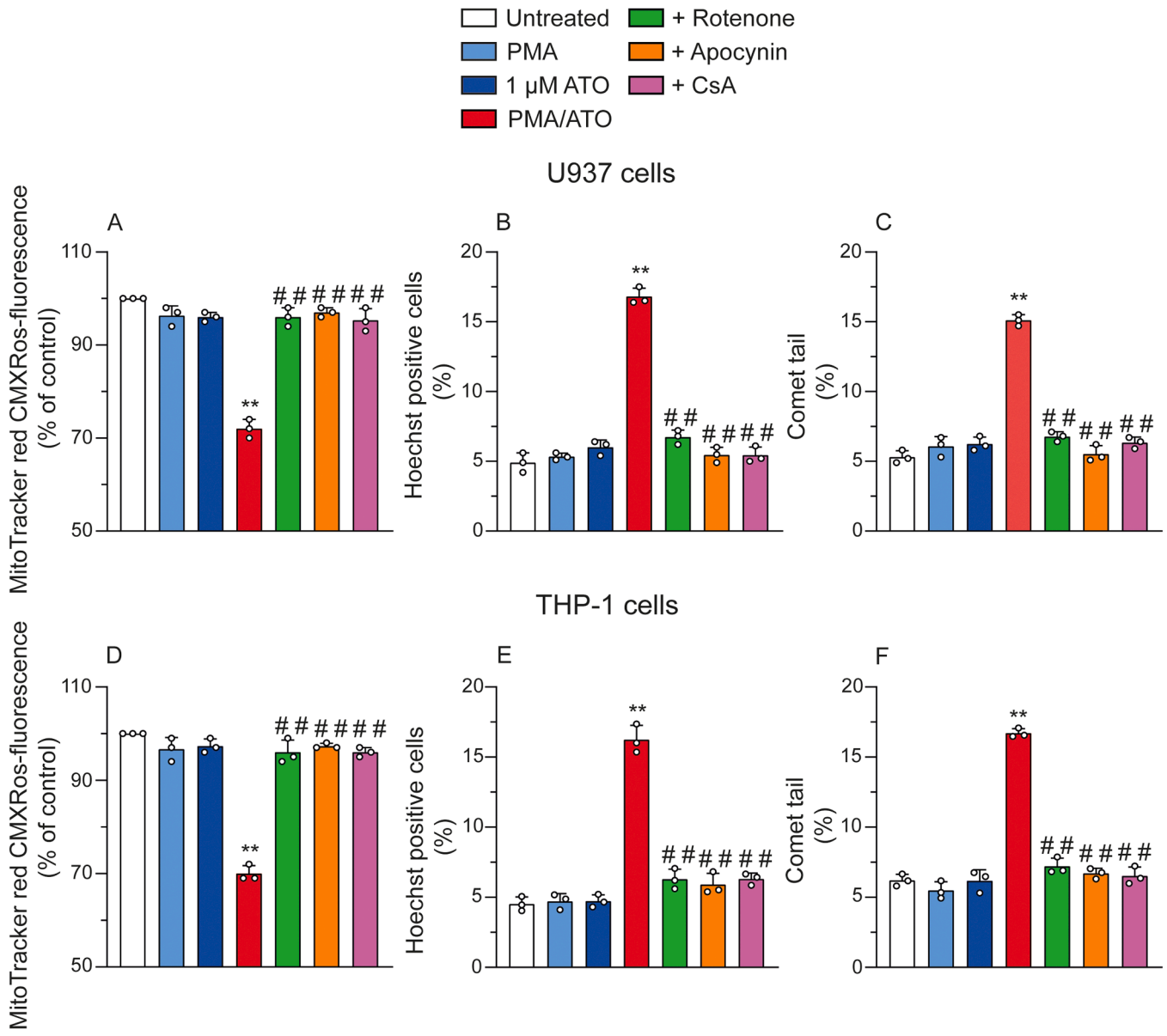

Fig. 8. PMA rescues ATO resistance to MPT-dependent apoptosis in U937 and THP-1 cells.U937 or THP-1 cells were pretreated for 5 min with the vehicle, rotenone, apocynin or CsA and incubated for 9 (A, D) or 14 (B, C, E, F) h with 1 μM ATO alone or associated with PMA. After treatments, the cells were analyzed for MitoTracker red CMXRos-fluorescence (A, D), and apoptotic DNA fragmentation/condensation by the Hoechst (B, E) or comet (C, F) assays. The results represent the means ± SD calculated from at least three distinct experiments. *P < 0.05, * *P < 0.01, compared with untreated cells. ##P < 0.01 compared with ATO/PMA treated cells (one-way ANOVA followed by Tukey test).

In resistant cells, the cocktail ATO/PMA also promoted the induction of a decline in mitochondrial potential, which, based on its sensitivity to CsA, is indicative of an ongoing MPT. Delayed induction of apoptotic DNA fragmentation/condensation was also detected under these conditions. The timing and inhibitor sensitivities of these events were identical to those detected in sensitive NB4 cells.

These results are therefore in keeping with the notion that AML cells are resistant to clinically relevant concentrations of ATO because of their poor NOX 2 dependent ROS response, insufficient for an effective downstream triggering of mito$O_2^{\cdot-}$ formation.

Our findings provide the conceptual basis to circumvent AML resistance to ATO with the use of clinically employed PMA analogues, as bryostatin [23]. A similar idea, however based on a different rationale, was put forward in a pioneer study of more than 20 years ago [23], which identified the pivotal role of NOX 2 activation in ATO induced NB4 cell killing. PMA and bryostatin, were shown to synergize with the

arsenic compound, thereby increasing its therapeutic potential. However, at least to our best knowledge, clinical studies using combined treatment with low concentrations of the two agents have never been performed. This was probably due to the significant therapeutic effects achieved by the currently employed ATO administration protocols, with manageable side effects for the patients [66,67]. Indeed, an array of cotreatments have been shown to increase ATO toxicity cells in *in vitro* studies, with very few of them being explored in a clinical setting [68].

Our results may renew interest in the use of ATO and a PMA analogue, with the aim of circumventing resistance of AML cells through the promotion of events associated with the triggering of the mitochondrial pathway of apoptosis.

A final issue addressed in this study was to compare the antioxidant status of APL and AML cells, as the intrinsic susceptibility of APL cells to ATO has been suggested to stem from weaker antioxidant defences [27,30,40]. This possibility, however, is not supported by the results of our experiments using $NaAsO_2$, which elicited in the three cell lines superimposable rates of mito$O_2^{\cdot-}$ emission. The similar MitoSOX red and DHR fluorescence responses detected under these conditions suggest equivalent antioxidant defences in both the cytosolic and mitochondrial compartments. Consistently, all three cell lines displayed similar levels of NPSH, GSH, catalase, and GPx, and accumulated equivalent DNA strand breaks in response to H_2O_2 exposure.

More perplexing, however, were the results regarding Nrf2-dependent antioxidant responses. In NB4 cells, exposure to 1 μM ATO significantly upregulated Nrf2 and its downstream target NQO1 *via* ROS-independent mechanisms, unaffected by rotenone or apocynin. Conversely, no such effect was observed in U937 or THP-1 cells under the same conditions. Although the ROS-independent activation of Nrf2 by ATO has been previously documented [69], the selective response of NB4 cells remains unexplained.

These findings are particularly intriguing because NB4 cells, despite their increased Nrf2 activation, remain highly susceptible to ATO-induced toxicity. This suggests that Nrf2 may have a dual role: while it is generally viewed as protective, in APL cells it might also contribute to their heightened sensitivity to ATO-induced oxidative stress. This phenomenon could be influenced by APL-specific factors, such as the PML-RARα oncoprotein or distinct stress response pathways. Further research is needed to clarify the precise mechanisms driving Nrf2 activation and its role in APL susceptibility.

In conclusion, the present study provides an explanation for the elevated susceptibility of APL cells to mito$O_2^{\cdot-}$ formation, and downstream MPT-dependent apoptosis, induced by clinically relevant concentrations of ATO. Under these conditions, the elevated NOX 2 dependent ROS response precedes and is critically connected with the formation of mitochondrial ROS. Resistance of AML cells to the same concentrations of ATO was based on their low NOX 2 dependent ROS response, unable to trigger the formation of mito$O_2^{\cdot-}$, and was therefore circumvented *via* direct NOX 2 stimulation with PMA. In addition, the antioxidant profiles of APL and AML cells were similar under baseline conditions, suggesting a weak link between this factor and the differing susceptibilities to ATO. However, clinically relevant concentrations of ATO uniquely stimulated the expression of Nrf2 and NQO1 in APL cells, an observation highlighting the need for further investigation to clarify the role of Nrf2 in APL's specific response to ATO.

CRediT authorship contribution statement

Andrea Guidarelli: Supervision, Methodology, Funding acquisition, Formal analysis, Data curation, Conceptualization. **Gloria Buffi:** Methodology, Formal analysis, Data curation. **Mara Fiorani:** Methodology, Formal analysis, Data curation. **Orazio Cantoni:** Writing – review & editing, Validation, Supervision, Project administration, Formal analysis, Data curation, Conceptualization. **Andrea Spina:** Methodology, Formal analysis, Data curation, Conceptualization.

Declaration of Competing Interest

The authors declare that they have no known competing financial interests or personal relationships that could have appeared to influence the work reported in this paper.

Acknowledgments

This work was supported by Ministero dell'Università e della Ricerca Scientifica e Tecnologica, Programmi di Ricerca Scientifica di Rilevante Interesse Nazionale, 2020, [Grant number: 2020ELYA32].

Appendix A. Supporting information

Supplementary data associated with this article can be found in the online version at doi:10.1016/j.phrs.2024.107554.

Data availability

The authors do not have permission to share data.

References

[1] M.A. Hussein, M. Saleh, F. Ravandi, J. Mason, R.M. Rifkin, R. Ellison, Phase 2 study of arsenic trioxide in patients with relapsed or refractory multiple myeloma, Br. J. Haematol. 125 (4) (2004) 470–476.
[2] G.J. Schiller, J. Slack, J.D. Hainsworth, J. Mason, M. Saleh, D. Rizzieri, D. Douer, A. F. List, Phase II multicenter study of arsenic trioxide in patients with myelodysplastic syndromes, J. Clin. Oncol. 24 (16) (2006) 2456–2464.
[3] G.J. Roboz, E.K. Ritchie, T. Curcio, J. Provenzano, R. Carlin, M. Samuel, B. Wittenberg, M. Mazumdar, P.J. Christos, S. Mathew, S. Allen-Bard, E.J. Feldman, Arsenic trioxide and low-dose cytarabine in older patients with untreated acute myeloid leukemia, excluding acute promyelocytic leukemia, Cancer 113 (9) (2008) 2504–2511.
[4] J. Zhou, R. Meng, X.H. Sui, L. Meng, B.F. Yang, Effects of arsenic trioxide administration styles on leukocytosis, Chin. Med. Sci. J. 21 (2) (2006) 111–114.
[5] G. Kchour, M. Tarhini, M.M. Kooshyar, H. El Hajj, E. Wattel, M. Mahmoudi, H. Hatoum, H. Rahimi, M. Maleki, H. Rafatpanah, S.A. Rezaee, M.T. Yazdi, A. Shirdel, H. de The, O. Hermine, R. Farid, A. Bazarbachi, Phase 2 study of the efficacy and safety of the combination of arsenic trioxide, interferon alpha, and zidovudine in newly diagnosed chronic adult T-cell leukemia/lymphoma (ATL), Blood 113 (26) (2009) 6528–6532.
[6] A. Emadi, S.D. Gore, Arsenic trioxide - an old drug rediscovered, Blood Rev. 24 (4-5) (2010) 191–199.
[7] J. Zhou, Y. Zhang, J. Li, X. Li, J. Hou, Y. Zhao, X. Liu, X. Han, L. Hu, S. Wang, Y. Zhao, Y. Zhang, S. Fan, C. Lv, L. Li, L. Zhu, Single-agent arsenic trioxide in the treatment of children with newly diagnosed acute promyelocytic leukemia, Blood 115 (9) (2010) 1697–1702.
[8] V. Mathews, B. George, K.M. Lakshmi, A. Viswabandya, A. Bajel, P. Balasubramanian, R.V. Shaji, V.M. Srivastava, A. Srivastava, M. Chandy, Single-agent arsenic trioxide in the treatment of newly diagnosed acute promyelocytic leukemia: durable remissions with minimal toxicity, Blood 107 (7) (2006) 2627–2632.
[9] R. Nasr, V. Lallemand-Breitenbach, J. Zhu, M.C. Guillemin, H. de The, Therapy-induced PML/RARA proteolysis and acute promyelocytic leukemia cure, Clin. Cancer Res. 15 (20) (2009) 6321–6326.
[10] S. Yousefnia, Mechanistic effects of arsenic trioxide on acute promyelocytic leukemia and other types of leukemias, Cell. Biol. Int. 45 (6) (2021) 1148–1157.
[11] V. Korsos, W.H. Miller Jr., How retinoic acid and arsenic transformed acute promyelocytic leukemia therapy, J. Mol. Endocrinol. 69 (4) (2022) T69–T83.
[12] W.H. Miller Jr., H.M. Schipper, J.S. Lee, J. Singer, S. Waxman, Mechanisms of action of arsenic trioxide, Cancer Res. 62 (14) (2002) 3893–3903.
[13] M. Yilmaz, H. Kantarjian, F. Ravandi, Acute promyelocytic leukemia current treatment algorithms, Blood Cancer J. 11 (6) (2021) 123.
[14] T.D. Zhang, G.Q. Chen, Z.G. Wang, Z.Y. Wang, S.J. Chen, Z. Chen, Arsenic trioxide, a therapeutic agent for APL, Oncogene 20 (49) (2001) 7146–7153.
[15] G.J. Roboz, S. Dias, G. Lam, W.J. Lane, S.L. Soignet, R.P. Warrell Jr., S. Rafii, Arsenic trioxide induces dose- and time-dependent apoptosis of endothelium and may exert an antileukemic effect via inhibition of angiogenesis, Blood 96 (4) (2000) 1525–1530.
[16] M. Yan, H. Wang, R. Wei, W. Li, Arsenic trioxide: applications, mechanisms of action, toxicity and rescue strategies to date, Arch. Pharm. Res. 47 (3) (2024) 249–271.
[17] Y. Ye, B. Gaugler, M. Mohty, F. Malard, Old dog, new trick: Trivalent arsenic as an immunomodulatory drug, Br. J. Pharmacol. 177 (10) (2020) 2199–2214.
[18] S. Shen, X.F. Li, W.R. Cullen, M. Weinfeld, X.C. Le, Arsenic binding to proteins, Chem. Rev. 113 (10) (2013) 7769–7792.

[19] J. Yi, F. Gao, G. Shi, H. Li, Z. Wang, X. Shi, X. Tang, The inherent cellular level of reactive oxygen species: one of the mechanisms determining apoptotic susceptibility of leukemic cells to arsenic trioxide, Apoptosis 7 (3) (2002) 209–215.
[20] S. Kumar, C.G. Yedjou, P.B. Tchounwou, Arsenic trioxide induces oxidative stress, DNA damage, and mitochondrial pathway of apoptosis in human leukemia (HL-60) cells, J. Exp. Clin. Cancer Res. 33 (1) (2014) 42.
[21] J. McCafferty-Grad, N.J. Bahlis, N. Krett, T.M. Aguilar, I. Reis, K.P. Lee, L.H. Boise, Arsenic trioxide uses caspase-dependent and caspase-independent death pathways in myeloma cells, Mol. Cancer Ther. 2 (11) (2003) 1155–1164.
[22] J. Dai, R.S. Weinberg, S. Waxman, Y. Jing, Malignant cells can be sensitized to undergo growth inhibition and apoptosis by arsenic trioxide through modulation of the glutathione redox system, Blood 93 (1) (1999) 268–277.
[23] W.C. Chou, C. Jie, A.A. Kenedy, R.J. Jones, M.A. Trush, C.V. Dang, Role of NADPH oxidase in arsenic-induced reactive oxygen species formation and cytotoxicity in myeloid leukemia cells, Proc. Natl. Acad. Sci. 101 (13) (2004) 4578–4583.
[24] X.H. Zhu, Y.L. Shen, Y.K. Jing, X. Cai, P.M. Jia, Y. Huang, W. Tang, G.Y. Shi, Y. P. Sun, J. Dai, Z.Y. Wang, S.J. Chen, T.D. Zhang, S. Waxman, Z. Chen, G.Q. Chen, Apoptosis and growth inhibition in malignant lymphocytes after treatment with arsenic trioxide at clinically achievable concentrations, J. Natl. Cancer Inst. 91 (9) (1999) 772–778.
[25] P. Westervelt, R.A. Brown, D.R. Adkins, H. Khoury, P. Curtin, D. Hurd, S.M. Luger, M.K. Ma, T.J. Ley, J.F. DiPersio, Sudden death among patients with acute promyelocytic leukemia treated with arsenic trioxide, Blood 98 (2) (2001) 266–271.
[26] N.J. Bahlis, J. McCafferty-Grad, I. Jordan-McMurry, J. Neil, I. Reis, M. Kharfan-Dabaja, J. Eckman, M. Goodman, H.F. Fernandez, L.H. Boise, K.P. Lee, Feasibility and correlates of arsenic trioxide combined with ascorbic acid-mediated depletion of intracellular glutathione for the treatment of relapsed/refractory multiple myeloma, Clin. Cancer Res. 8 (12) (2002) 3658–3668.
[27] Y. Jing, J. Dai, R.M. Chalmers-Redman, W.G. Tatton, S. Waxman, Arsenic trioxide selectively induces acute promyelocytic leukemia cell apoptosis via a hydrogen peroxide-dependent pathway, Blood 94 (6) (1999) 2102–2111.
[28] S. Korper, F. Nolte, E. Thiel, H. Schrezenmeier, M.T. Rojewski, The role of mitochondrial targeting in arsenic trioxide-induced apoptosis in myeloid cell lines, Br. J. Haematol. 124 (2) (2004) 186–189.
[29] L. Li, J. Wang, R.D. Ye, G. Shi, H. Jin, X. Tang, J. Yi, PML/RARalpha fusion protein mediates the unique sensitivity to arsenic cytotoxicity in acute promyelocytic leukemia cells: mechanisms involve the impairment of cAMP signaling and the aberrant regulation of NADPH oxidase, J. Cell Physiol. 217 (2) (2008) 486–493.
[30] J. Wang, L. Li, H. Cang, G. Shi, J. Yi, NADPH oxidase-derived reactive oxygen species are responsible for the high susceptibility to arsenic cytotoxicity in acute promyelocytic leukemia cells, Leuk. Res. 32 (3) (2008) 429–436.
[31] R.K. Srivastava, C. Li, A. Ahmad, O. Abrams, M.S. Gorbatyuk, K.S. Harrod, R. C. Wek, F. Afaq, M. Athar, ATF4 regulates arsenic trioxide-mediated NADPH oxidase, ER-mitochondrial crosstalk and apoptosis, Arch. Biochem. Biophys. 609 (2016) 39–50.
[32] R.P. Brandes, N. Weissmann, K. Schroder, Nox family NADPH oxidases: molecular mechanisms of activation, Free Radic. Biol. Med. 76 (2014) 208–226.
[33] K. Bedard, K.H. Krause, The NOX family of ROS-generating NADPH oxidases: physiology and pathophysiology, Physiol. Rev. 87 (1) (2007) 245–313.
[34] I. Aldoss, L. Mark, J. Vrona, L. Ramezani, I. Weitz, A.M. Mohrbacher, D. Douer, Adding ascorbic acid to arsenic trioxide produces limited benefit in patients with acute myeloid leukemia excluding acute promyelocytic leukemia, Ann. Hematol. 93 (11) (2014) 1839–1843.
[35] A.M. Ramos, C. Fernandez, D. Amran, P. Sancho, E. de Blas, P. Aller, Pharmacologic inhibitors of PI3K/Akt potentiate the apoptotic action of the antileukemic drug arsenic trioxide via glutathione depletion and increased peroxide accumulation in myeloid leukemia cells, Blood 105 (10) (2005) 4013–4020.
[36] Y. Sanchez, D. Amran, C. Fernandez, E. de Blas, P. Aller, Genistein selectively potentiates arsenic trioxide-induced apoptosis in human leukemia cells via reactive oxygen species generation and activation of reactive oxygen species-inducible protein kinases (p38-MAPK, AMPK), Int. J. Cancer 123 (5) (2008) 1205–1214.
[37] M.C. Estan, E. Calvino, S. Calvo, B. Guillen-Guio, C. Boyano-Adanez Mdel, E. de Blas, E. Rial, P. Aller, Apoptotic efficacy of etomoxir in human acute myeloid leukemia cells. Cooperation with arsenic trioxide and glycolytic inhibitors, and regulation by oxidative stress and protein kinase activities, PLoS One 9 (12) (2014) e115250.
[38] M.C. Estan, E. Calvino, E. de Blas, C. Boyano-Adanez Mdel, M.L. Mena, M. Gomez-Gomez, E. Rial, P. Aller, 2-Deoxy-D-glucose cooperates with arsenic trioxide to induce apoptosis in leukemia cells: involvement of IGF-1R-regulated Akt/mTOR, MEK/ERK and LKB-1/AMPK signaling pathways, Biochem. Pharmacol. 84 (12) (2012) 1604–1616.
[39] G.Q. Chen, J. Zhu, X.G. Shi, J.H. Ni, H.J. Zhong, G.Y. Si, X.L. Jin, W. Tang, X.S. Li, S.M. Xong, Z.X. Shen, G.L. Sun, J. Ma, P. Zhang, T.D. Zhang, C. Gazin, T. Naoe, S. J. Chen, Z.Y. Wang, Z. Chen, In vitro studies on cellular and molecular mechanisms of arsenic trioxide (As_2O_3) in the treatment of acute promyelocytic leukemia: As_2O_3 induces NB4 cell apoptosis with downregulation of Bcl-2 expression and modulation of PML-RAR alpha/PML proteins, Blood 88 (3) (1996) 1052–1061.
[40] X. Cai, Y.L. Shen, Q. Zhu, P.M. Jia, Y. Yu, L. Zhou, Y. Huang, J.W. Zhang, S. M. Xiong, S.J. Chen, Z.Y. Wang, Z. Chen, G.Q. Chen, Arsenic trioxide-induced apoptosis and differentiation are associated respectively with mitochondrial transmembrane potential collapse and retinoic acid signaling pathways in acute promyelocytic leukemia, Leukemia 14 (2) (2000) 262–270.
[41] Y.C. Mun, J.Y. Ahn, E.S. Yoo, K.E. Lee, E.M. Nam, J. Huh, H.A. Woo, S.G. Rhee, C. M. Seong, Peroxiredoxin 3 has important roles on arsenic trioxide induced apoptosis in human acute promyelocytic leukemia cell line via hyperoxidation of mitochondrial specific reactive oxygen species, Mol. Cells 43 (9) (2020) 813–820.
[42] D. Darr, I. Fridovich, Irreversible inactivation of catalase by 3-amino-1,2,4-triazole, Biochem. Pharmacol. 35 (20) (1986) 3642.
[43] P. Mukhopadhyay, M. Rajesh, G. Hasko, B.J. Hawkins, M. Madesh, P. Pacher, Simultaneous detection of apoptosis and mitochondrial superoxide production in live cells by flow cytometry and confocal microscopy, Nat. Protoc. 2 (9) (2007) 2295–2301.
[44] N. Atale, S. Gupta, U.C. Yadav, V. Rani, Cell-death assessment by fluorescent and nonfluorescent cytosolic and nuclear staining techniques, J. Microsc. 255 (1) (2014) 7–19.
[45] I. Schmid, C. Uittenbogaart, B.D. Jamieson, Live-cell assay for detection of apoptosis by dual-laser flow cytometry using Hoechst 33342 and 7-amino-actinomycin D, Nat. Protoc. 2 (1) (2007) 187–190.
[46] N.P. Singh, M.T. McCoy, R.R. Tice, E.L. Schneider, A simple technique for quantitation of low levels of DNA damage in individual cells, Exp. Cell Res. 175 (1) (1988) 184–191.
[47] O. Cantoni, A. Guidarelli, Indirect mechanisms of DNA strand scission by peroxynitrite, Methods Enzym. 440 (2008) 111–120.
[48] M. Fiorani, A. Guidarelli, V. Capellacci, L. Cerioni, R. Crinelli, O. Cantoni, The dual role of mitochondrial superoxide in arsenite toxicity: signaling at the boundary between apoptotic commitment and cytoprotection, Toxicol. Appl. Pharmacol. 345 (2018) 26–35.
[49] S. Brundu, L. Palma, G.G. Picceri, D. Ligi, C. Orlandi, L. Galluzzi, L. Chiarantini, A. Casabianca, G.F. Schiavano, M. Santi, F. Mannello, K. Green, M. Smietana, M. Magnani, A. Fraternale, Glutathione depletion is linked with Th2 polarization in mice with a retrovirus-induced immunodeficiency syndrome, murine AIDS: role of proglutathione molecules as immunotherapeutics, J. Virol. 90 (16) (2016) 7118–7130.
[50] E. Beutler. Red cell metabolism: a manual of biochemical methods, 3rd ed., Grune & Stratton Orlando, FL, 1984.
[51] A. Gomes, E. Fernandes, J.L. Lima, Fluorescence probes used for detection of reactive oxygen species, J. Biochem. Biophys. Methods 65 (2-3) (2005) 45–80.
[52] M. Degli Esposti, Inhibitors of NADH-ubiquinone reductase: an overview, Biochim. Biophys. Acta 1364 (2) (1998) 222–235.
[53] A. Guidarelli, A. Catalani, A. Spina, E. Varone, S. Fumagalli, E. Zito, M. Fiorani, O. Cantoni, Functional organization of the endoplasmic reticulum dictates the susceptibility of target cells to arsenite-induced mitochondrial superoxide formation, mitochondrial dysfunction and apoptosis, Food Chem. Toxicol. 156 (2021) 112523.
[54] R. Takeya, N. Ueno, K. Kami, M. Taura, M. Kohjima, T. Izaki, H. Nunoi, H. Sumimoto, Novel human homologues of p47phox and p67phox participate in activation of superoxide-producing NADPH oxidases, J. Biol. Chem. 278 (27) (2003) 25234. -2546.
[55] G. Paradies, G. Petrosillo, V. Paradies, F.M. Ruggiero, Role of cardiolipin peroxidation and Ca^{2+} in mitochondrial dysfunction and disease, Cell Calcium 45 (6) (2009) 643–650.
[56] A.P. Halestrap, C.P. Connern, E.J. Griffiths, P.M. Kerr, Cyclosporin A binding to mitochondrial cyclophilin inhibits the permeability transition pore and protects hearts from ischaemia/reperfusion injury, Mol. Cell Biochem. 174 (1-2) (1997) 167–172.
[57] S. Dikalov, Cross talk between mitochondria and NADPH oxidases, Free Radic. Biol. Med. 51 (7) (2011) 1289–1301.
[58] S. Kröller-Schön, S. Steven, S. Kossmann, A. Scholz, S. Daub, M. Oelze, N. Xia, M. Hausding, Y. Mikhed, E. Zinssius, M. Mader, P. Stamm, N. Treiber, K. Scharffetter-Kochanek, H.G. Li, E. Schulz, P. Wenzel, T. Münzel, A. Daiber, Molecular mechanisms of the crosstalk between mitochondria and NADPH oxidase through reactive oxygen species-studies in white blood cells and in animal models, Antioxid. Redox Sign. 20 (2) (2014) 247–266.
[59] N. Koju, A. Taleb, J. Zhou, G. Lv, J. Yang, X. Cao, H. Lei, Q. Ding, Pharmacological strategies to lower crosstalk between nicotinamide adenine dinucleotide phosphate (NADPH) oxidase and mitochondria, Biomed. Pharmacother. 111 (2019) 1478–1498.
[60] A. Guidarelli, L. Cerioni, M. Fiorani, A. Catalani, O. Cantoni, Arsenite-induced mitochondrial superoxide formation: time and concentration requirements for the effects of the metalloid on the endoplasmic reticulum and mitochondria, J. Pharmacol. Exp. Ther. 373 (1) (2020) 62–71.
[61] A. Guidarelli, A. Spina, G. Buffi, G. Blandino, M. Fiorani, O. Cantoni, ERO1alpha primes the ryanodine receptor to respond to arsenite with concentration dependent Ca^{2+} release sequentially triggering two different mechanisms of ROS formation, Chem. Biol. Interact. 383 (2023) 110694.
[62] P.R. Angelova, A.Y. Abramov, Functional role of mitochondrial reactive oxygen species in physiology, Free Radic. Biol. Med. 100 (2016) 81–85.
[63] A.V. Kudryavtseva, G.S. Krasnov, A.A. Dmitriev, B.Y. Alekseev, O.L. Kardymon, A. F. Sadritdinova, M.S. Fedorova, A.V. Pokrovsky, N.V. Melnikova, A.D. Kaprin, A. A. Moskalev, A.V. Snezhkina, Mitochondrial dysfunction and oxidative stress in aging and cancer, Oncotarget 7 (29) (2016) 44879–44905.
[64] D.B. Zorov, M. Juhaszova, S.J. Sollott, Mitochondrial reactive oxygen species (ROS) and ROS-induced ROS release, Physiol. Rev. 94 (3) (2014) 909–950.
[65] H. Sies, D.P. Jones, Reactive oxygen species (ROS) as pleiotropic physiological signalling agents, Nat. Rev. Mol. Cell Biol. 21 (7) (2020) 363–383.
[66] Q.Q. Wang, H.Y. Hua, H. Naranmandura, H.H. Zhu, Balance between the toxicity and anticancer activity of arsenic trioxide in treatment of acute promyelocytic leukemia, Toxicol. Appl. Pharmacol. 409 (2020) 115299.

[67] P. Zhang, On arsenic trioxide in the clinical treatment of acute promyelocytic leukemia, Leuk. Res. Rep. 7 (2017) 29–32.
[68] Y. Jiang, X. Shen, F. Zhi, Z. Wen, Y. Gao, J. Xu, B. Yang, Y. Bai, An overview of arsenic trioxide-involved combined treatment algorithms for leukemia: basic concepts and clinical implications, Cell Death Discov. 9 (1) (2023) 266.
[69] A.A. Morales, D. Gutman, P.J. Cejas, K.P. Lee, L.H. Boise, Reactive oxygen species are not required for an arsenic trioxide-induced antioxidant response or apoptosis, J. Biol. Chem. 284 (19) (2009) 12886–12895.